Journal of Hydrology 601 (2021) 126706

Contents lists available at ScienceDirect

Journal of Hydrology

journal homepage: www.elsevier.com/locate/jhydrol

# Sensitivity analysis of hydrological processes to perturbed climate in a southern boreal forest basin

Zhihua He [a,b,*], John W. Pomeroy [a,b], Xing Fang [a,b], Amber Peterson [b]

[a] Centre for Hydrology, University of Saskatchewan, Canada
[b] Global Institute for Water Security, University of Saskatchewan, Canada

ARTICLE INFO

This manuscript was handled by Jiri Simunek, Editor-in-Chief, with the assistance of Habib Basha, Associate Editor

*Keywords:*
Boreal forest basin
CRHM-created Boreal Hydrology Model
Sensitivities of hydrological processes
Perturbed precipitation and temperature

ABSTRACT

Hydrological processes over and through frozen and unfrozen ground were simulated in the well instrumented boreal forest basin of White Gull Creek, Saskatchewan, Canada using a model created using the flexible Cold Regions Hydrological Modelling (CRHM) platform. The CRHM-created Boreal Hydrology Model was structured and initially parameterized using decades of process hydrology research in the southern boreal forest with minor parameter calibration, and generally produced quite good performance on simultaneously reproducing the measurements of runoff, snow water equivalent (SWE), soil liquid water content and eddy correlation flux tower observations of evapotranspiration (ET) over two decades. To examine the sensitivity of basin hydrology to perturbed climate inputs, air temperature (T) inputs were set up by linear increments in the reference observation of up to +6 ℃, and precipitation (P) inputs were generated by multiplying the reference observed P from 70% to 130%. The model results showed that the basin hydrological variables showed quite different sensitivities to perturbations of P and T. The volume of annual runoff and the annual runoff coefficient increased more rapidly with rising P, at rates of 31% and 16% per 10% increase in P, but decreased by only 3.8% and 4.7% per 1 ℃ of warming. Annual ET increased rapidly with temperature, by 7% per 1 ℃ of warming and therefore drove the streamflow volumetric changes with warming, but increased only 1% per 10% increase in P. Perturbations of P and T had distinctively different influences on the streamflow regime. Increased P enhanced the intra- and inter-annual variabilities of basin runoff, reduced the relative contribution of winter runoff to annual runoff and increased the relative contribution of summer runoff; whilst rising T resulted in the inverse changes in the streamflow regime. Effects of warming on some hydrological processes could be compensated for to varying degrees by the effects of increases in P. Reductions in the annual runoff volume and runoff coefficient caused by warming up to 6 ℃ could be compensated for by increases of <20% in P. However, the maximum increase in P (+30%) examined could only compensate for the changes in snow processes caused by warming of less than 4 ℃ and snow-cover duration decreases with 1 ℃ warming could not be compensated for by any precipitation increase considered. These results inform the vulnerability of boreal forest hydrology to the first-order changes in P and T and provide guidance for further climate impact assessments for hydrology in the southern boreal forest in Canada.

## 1. Introduction

The boreal zone covers the northern high latitudes in North America and Eurasia, about 28% of which is in Canada, spanning from the international border between Yukon and Alaska to Newfoundland and Labrador (Brandt et al., 2013). The boreal forest that dominates this zone is approximately one third of the global forested area (Gauthier et al., 2015) and plays an important role in the hydrology of northern rivers in the circumpolar North (Buttle et al., 2000). Boreal forests are currently experiencing more severe climate change than the global average (Price et al., 2013), and this is expected to continue in the future. One reason for the stronger climatic change in boreal zones is the reduced surface albedo caused by reduced snow cover (Bonan, 2008; Euskirchen et al., 2010; Kozii et al., 2017). Recent analyses from Environment and Climate Change Canada reported by Bush and Lemmen (2019) suggest median temperature (T) and annual precipitation (P) increases of 2.3 °C and 7.5% respectively for the period 2031–2050 and 6.4 °C and 18.4% respectively for 2081–2100 under RCP8.5, compared

* Corresponding author.
*E-mail address:* zhh624@mail.usask.ca (Z. He).

https://doi.org/10.1016/j.jhydrol.2021.126706
Received 22 February 2021; Received in revised form 19 June 2021; Accepted 13 July 2021
Available online 19 July 2021

to 1986–2005. Such changes in T and P are magnified in winter and so could have strong effects on the snow accumulation and losses, as well as other hydrological processes in boreal forest (Kozii et al., 2017). However, the sensitivities of hydrological processes to climate changes in boreal forest are less well understood in comparison to warmer regions in Canada (Buttle and Metcalfe, 2000; Metcalfe and Buttle, 2001).

The boreal forest is characterized by a long and cold winter (Hardy et al., 1998; Nelson et al., 2014). Snow mass and energy balance in the forest are regulated by the canopy through multiple processes such as interception and sublimation of snowfall, reduced shortwave radiation, and enhanced longwave radiation from the forest trunk (Pomeroy et al., 1998; Pomeroy et al., 2009; Ellis et al., 2010; Rasmus et al., 2013). Higher canopy coverage typically results in increased snow interception and snow sublimation, as well as slower snowmelt below the mature boreal forests (Pomeroy and Granger, 1997; Hedstrom and Pomeroy, 1998; Kozii et al., 2017; Pomeroy et al., 2002; Gelfan et al., 2004). As a result, winter snow accumulation under mature boreal forests that are dominated by needleleaf trees is substantially lower than that in adjacent clearings or deciduous forest stands (Pomeroy and Gray, 1995). Snow and forest cover also influence the seasonal freezing of soils and spring snowmelt infiltration to and runoff over frozen soils (Gray et al., 2001). The strong effects of forest canopy on snow accumulation and snowmelt in turn dictate the complexity in the runoff generation processes.

However, boreal forests are typically remote and extensive (Sulla-Menashe et al., 2018), creating great challenges for surface observations of its hydrometeorological characteristics. For example, Brown et al. (2019) demonstrated a lower density of snow observation in the boreal forest than those in the Prairies and western mountains in Canada. The strong spatial variability of snow accumulation across forest and open clearing sites impairs the representativeness of point or small-area snow surveys for estimates at a basin scale (Pomeroy et al., 2002). Empirical snowmelt models that need detailed field measurements for temperature-index melt parameter calibration have limited predictive capability in the boreal forest basins where stand snow density varies substantially, and calibration datasets are often unavailable (Ellis et al., 2010). A physically based cold regions hydrological model which requires minor to no parameter calibration by field measurements is needed to capture the complicated runoff processes for boreal forests (Pomeroy et al., 1999).

Changes in T and P cause distinctive changes in the operation of hydrological processes in boreal forest ecosystem. Rising T generally leads to increasing evapotranspiration and reduces soil water availability for tree growth in boreal forests (Granger and Pomeroy, 1997; Elliott et al., 1998; Peng et al., 2011); whilst increasing P has the potential to compensate for reduced water availability caused by rising T. However, to what extent the effect of warming T on water availability could be compensated for by increasing P has not been evaluated in boreal forest river basins. Climate change scenarios simulated by global and regional climate models (GCM and RCM) contain large uncertainties for future hydroclimates due to coarse spatial resolution, non-explicit parameterisation of convective storms (Li et al., 2019), and low capability to capture the effects of sub-grid features of precipitation dynamics and land cover feedbacks (Rasouli et al., 2014; Rasouli et al., 2019). Alternatively, linear changes of P and T, produced by perturbing the current observed time series of P and T from instrumented basins up to the corresponding change ranges projected by an ensemble of climate models have been demonstrated as highly suited to investigate the hydrological sensitivity to climate change and the compensation effects between P and T perturbations in cold regions (e.g. Rasouli et al., 2014; Rasouli et al., 2015; Aygün et al., 2020; He, 2021).

In light of this background, the objective of this paper is to investigate the sensitivities of hydrological processes in a boreal forest drainage basin to P and T perturbations. The specific research questions are threefold:

(1) Can the full range of boreal forest hydrological processes be represented in a physically based hydrological model with minimal parameter calibration?

(2) How is basin hydrology in the boreal forest sensitive to a wide range of perturbations of P and T?

(3) To what extent can the effects of warming T on hydrological processes in the boreal forest be compensated for by increased precipitation?

The questions will be addressed using perturbed P and T simulations made with a physically based hydrological model that is suitable for cold regions boreal forest hydrology and was tested in a well instrumented boreal forest research basin.

## 2. Study area and data

The study was conducted in the White Gull Creek (WGC), a boreal forest basin located in central Saskatchewan, in the southern Canadian boreal forest (Fig. 1). The basin has an effective drainage area of 603 $km^2$, with elevations ranging from 472 m a.s.l. (above sea level) to 688 m a.s.l., and is covered by four forest types: harvested jack pine (HJP, 33.4 $km^2$), old jack pine (OJP, 67.2 $km^2$), aspen (ASP, 137.3 $km^2$) and old black spruce (OBS, 254.1 $km^2$). The remaining basin area is covered by open wetland (Fen, 94.2 $km^2$) and open water bodies (16.4 $km^2$). Annual mean P and T are 440 mm (around 30% as snow) and 1.5 ℃, respectively, during the period of 1998–2016 measured at the OBS station by Environment and Climate Change Canada. The basin surficial geology is mainly composed of Pleistocene and Holocene glacial deposits (Nijssen and Lettenmaier, 2002). Soil textures in the basin mainly consist of loam, sand and clay (Agriculture and Agri-Food Canada, 2015). The organic layer depth is generally 8–10 cm (Bartlett et al., 2006).

Intensive observations started with the Boreal Ecosystem-Atmosphere Study (BOREAS) in 1993 (Sellers et al., 1997) which later became the Government of Canada's and the University of Saskatchewan's Boreal Ecosystem Research and Monitoring Sites (BERMS). Double scaffold towers (with heights of around 26 m, stretching to approximately twice height of the canopy) equipped with meteorological and flux instrumentations (such as Vaisala HMP45 and RM Young T/RH in radiation shield, RM Young 05103 wind monitor and RM Young cup anemometer) have been operated on the OJP and OBS sites since 1997. Meteorological datasets, including P, T, wind speed, relative humidity, carbon and water flux, and solar radiation, were measured every 30-minute at the OBS and OJP stations (Fig. 1). Precipitation was measured by a Geonor T-200B weighing precipitation gauge and a CS700 tipping bucket rain gauge. Missing data were infilled using measurements from nearby BERMS weather stations based on regression relations that were developed on overlapping measurement periods (Davison et al., 2016). Instruments for the measurements of multiple variables are presented in Table 1.

Soil liquid volume water content (VWC) observations at multiple depths (0–15 cm, 15–30 cm, 30–60 cm and 60–90 cm) have been recorded by the CS615 water content reflectometer and CS616 TDR sensor every 4 h at the OBS and OJP sites since 1997. Evapotranspiration (ET) was measured using an eddy-covariance system and method every 30-minutes. The eddy-covariance system consists of a CSAT3 sonic anemometer that measures wind speed in three dimensions and a LI-7200 infrared gas analyzer. The EC system measured sensible and latent heat fluxes and net ecosystem exchange based on the changes of eddy fluxes and storage in the air underneath the EC system (Barr et al., 2012). An energy-closure factor calculated from the measured energy fluxes was used to estimate an energy-closure adjusted ET. To convert to mm of water, latent heat of vaporizations of 2.83 and 2.45 MJ/kg were used during the sublimation period and rainy period, respectively. Continuous snow depth at a point near the tower was measured with Campbell Scientific Canada SR50 and SR50-AT sonic rangers. Periodic winter and spring snow surveys have been taken on transects near the OBS and OJP sites since 1993. At each survey transect, 5 density

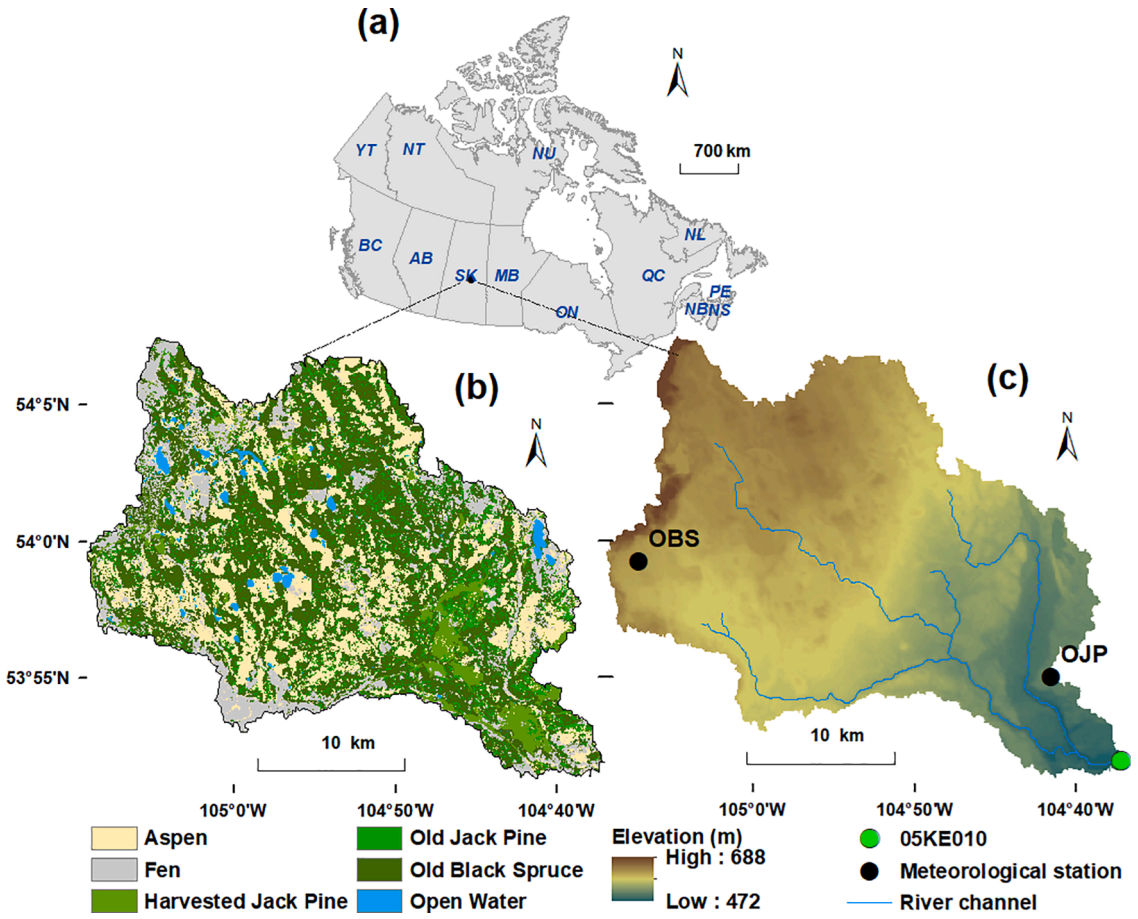


**Fig. 1.** (a) Location of the White Gull Creek basin in Canada, (b) land cover types, and (c) elevations and stations. OBS and OJP refer to the meteorological stations and sites for snow and soil moisture surveys.

**Table 1**
Instruments for field measurements in the White Gull Creek basin.

| Variable | Equipment/Sensor | Sampling Frequency | Sites |
|---|---|---|---|
| Snow water equivalent (SWE) | SR50 and SR50-AT sonic rangers, and snow stakes | Couple of times each year | OJP and OBS |
| Evapotranspiration (ET) | eddy-covariance system with CSAT3 sonic anemometer and LI-7200 infrared gas analyzer | 30-min | OJP and OBS |
| Soil liquid volume water content (VWC) | CS615 water content reflectometer and CS616 TDR sensor | 4-h | OJP and OBS |
| Meteorology (P, T, Relative humidity, radiation, and wind speed) | Double scaffold tower equipped with multiple sensors such as Vaisala HMP45 and RM Young T/RH in radiation shield; RM Young 05103 wind monitor and RM Young cup anemometer; CNR1 net radiometer and LI-190 quantum sensor; Geonor T-200B and CS700 rain gauge. | 30-min | OJP and OBS |
| Streamflow | N/A | daily | 05KE010, at high way No. 106 |

measurements and 45 depth measurements were taken along a 100 m survey line. Averaged snow depths and densities measurements were used to estimate the mean snow water equivalent (SWE) at the survey transect as per Pomeroy and Gray (1995).

Daily streamflow data have been collected at a hydrometric station (05KE010, 104.62° W and 53.86° N) located at the outlet of White Gull Creek by the Environment and Climate Change Canada's Water Survey of Canada since 1993. Water level data were measured at used along with manually measured depth-discharge rating curves to estimate streamflow discharge at daily timesteps, continuously through January to December. A full description of the sites, forest and data available can be found here https://water.usask.ca/berms/index.php and a description of water balance variables and streamflow is provided by Barr et al. (2012). The meteorological, flux, and soil data are available at: https://doi.org/10.20383/101.0292 (Ahmed et al., 2020).

## 3. Methodology

### 3.1. Hydrological model

A physically based hydrological model, the Boreal Hydrology Model, was set up for the WGC basin using the Cold Regions Hydrological Modelling (CRHM) platform. CRHM is an object-oriented platform for assembling hydrological modules. The user constructs a purpose-built hydrological model with CRHM by selecting modules that are suitable for the spatial configurations and physical hydrological processes in the basin of interest. Hydrological response units (HRUs) are used to discretize the basin and are determined based on variability of basin attributes and level of physical complexity chosen for the model. Physical

complexity is decided by the user, given the data availability, hydrological complexity, and the objective flux or state for prediction. Pomeroy et al. (2007) provided a full description of CRHM, including evaluation of some of its modules using BERMS data. Updates to the model for forest hydrology are provided by Ellis et al. (2010) and Pomeroy et al. (2012). Fig. 2 shows the schematic setup of physically based modules that were constructed in WGC basin, which include:

1. Solar radiation: estimates maximum sunshine hours, direct and diffuse solar radiation according to basin characteristics of latitude, altitude, azimuth and terrain slope (Garnier and Ohmura, 1970).
2. Observation: reads the time series of T, wind speed, relative humidity and P, and estimates spatial distributions of T, humidity, P and P phase with adjustments for elevation to downscale to each HRU (Harder and Pomeroy, 2013).
3. Sunshine hour: calculates sunshine hours for HRUs from solar irradiance observations.
4. Longwave radiation: estimates longwave radiation using shortwave irradiance from the solar radiation module (Sicart et al., 2006).
5. Slope radiation: calculates shortwave irradiance to HRU slope using estimate of the solar radiation module.
6. Canopy: calculates interceptions of snowfall and rainfall, snow sublimation, evaporation of intercepted rainfall, drip and unloading water from the forest canopy, and thus updates the snowfall, rainfall, shortwave and longwave irradiance under the canopy (Ellis et al., 2010).
7. Albedo (Verseghy, 1991): calculates surface albedos of snow covered and snow-free surfaces for the summer net radiation and energy-balance snowmelt modules.
8. Blowing snow (Pomeroy and Li, 2000): estimates inter-HRU snow transports and blowing snow sublimation losses forced by wind in the snow accumulation period using a version of the Prairie Blowing Snow Model (Pomeroy et al., 1993).
9. Energy-balance snowmelt: estimates energy balance of radiation, latent and sensible heats, ground heat, rainfall advection, and the internal energy exchanges across snowpack layers, and calculates the snowmelt and runoff through snowpack using a version of the Snobal model (Marks et al., 1998).
10. Summer net radiation (Granger and Gray, 1990): estimates net radiation from short and long-wave radiations for the ground surface T and evaporation modules in the snow-free season.
11. Ground surface T: estimates T of the ground surface using the radiative-conductive-convective approach in Williams et al. (2015). Air T, thermal conductivity, energy balance of snowpack in the snow covered period and net radiation in the snow-free period were used as inputs (Luce and Tarboton 2010).
12. Volumetric soil moisture: converts soil moisture depths from the soil module to volumetric soil moisture and initializes the fall soil saturation status for the infiltration module.
13. Infiltration: calculates snowmelt infiltration into frozen soils using Gray's parametric infiltration algorithm (Zhao and Gray, 1999; Gray et al., 2001) and rainfall infiltration into unfrozen soils using Ayers' infiltration scheme (Ayers, 1959). This module permits infiltration to soil column by linking with the soil module, and computes surface runoff when snowmelt or rainfall exceeds the infiltration rate (infiltration excess runoff).
14. Thaw-freeze fronts (Changwei and Gough, 2013): simulates the seasonal freezing and thawing fronts in frost based on ground surface T using a modified Stefan's heat flow equation.
15. Evaporation: estimates actual evapotranspiration from unsaturated surfaces using the Penman-Monteith (P-M) evapotranspiration algorithm (Monteith, 1965) with a Jarvis-style resistance formulation (Verseghy, 1991). The Priestley and Taylor evaporation expression (Priestley and Taylor, 1972) was used to estimate evaporation from saturated surfaces of open water bodies, wetlands and river channels. Both evaporation algorithms are restricted by water availability, and subsequently update water storages in the interception and depression stores and soil layers.
16. Soil moisture: simulates groundwater-surface water interactions and calculates subsurface interflow from soil water and deep groundwater flow, updating water storages in surface depressions, soil layers and groundwater aquifer (Fang et al., 2010;

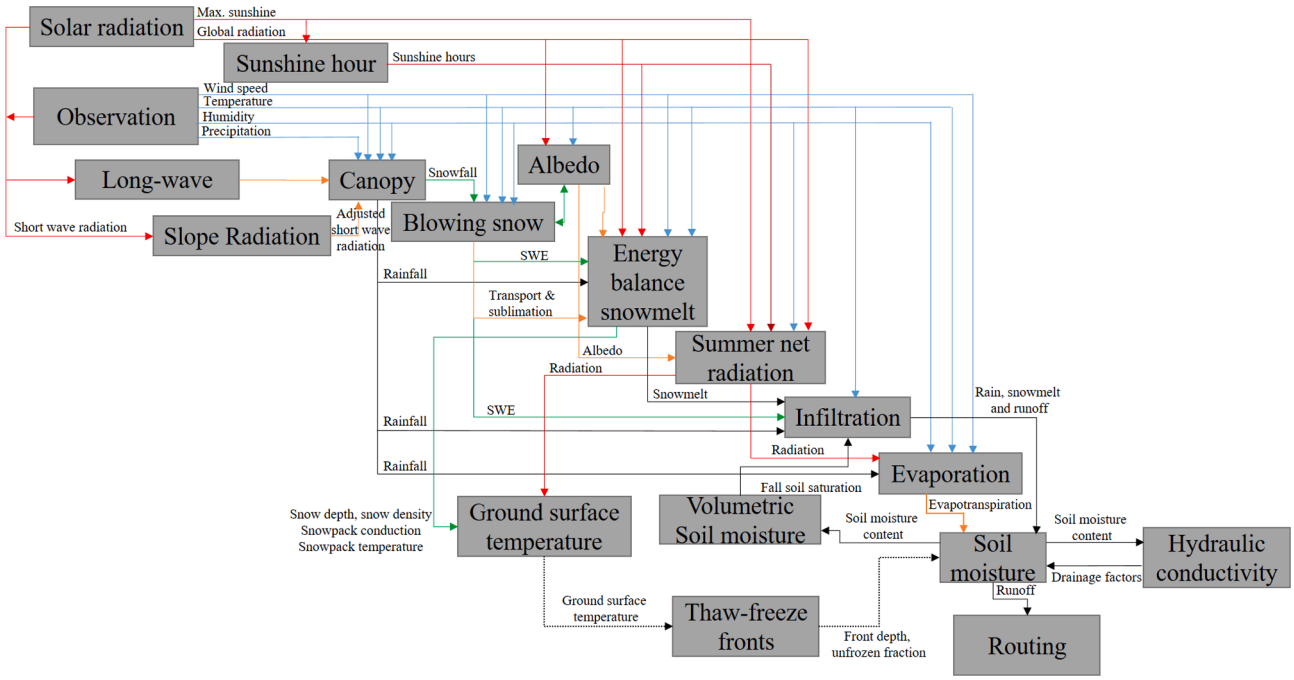


**Fig. 2.** Module structure of the physically based hydrological model for White Gull Creek basin, including process and data modules and flow of variables for radiation (red line), meteorology (blue line), evaporation and sublimation (orange line), snow (green line) and soil moisture content, ground surface temperature and water (black line).

Fang et al., 2013; Pomeroy et al., 2016). Thawing and freezing fronts simulated by the thaw-freeze front module are presented in soil layers to regulate the moisture movement.

17. Hydraulic conductivity: estimates drainage factors in soil layers and groundwater layer based on Darcy's law for unsaturated hydraulic conductivity (Fang et al., 2013; Pomeroy et al., 2016).
18. Routing: uses the Muskingum method (Chow, 1964) to route runoff between HRUs and the Clark's lag and route algorithm (Clark, 1945) for subsurface interflow and groundwater flow.

In WGC, six HRUs were used to discretize the basin based on the land cover types: open water and channel, HJP, OJP, ASP, OBS, and Fen shown in Fig. 1 and Table 2. Meteorological forcing data for the HRUs were estimated by lapse rates derived from the observations at the OJP and OBS sites. The simulation was conducted for 19 years starting from 1998 to 2016. The Boreal Hydrological Model performance for the simulations of runoff, snow water equivalent (SWE), soil liquid water content (VWC) and evapotranspiration were examined by four statistical metrics: Nash–Sutcliffe efficiency (NSE) (Nash and Sutcliffe, 1970), logarithmic NSE (logNSE), model bias (MB), and normalized root mean square error (NRMSE).

$$\mathrm{NSE} = 1 - \frac{\sum (X_o - X_s)^2}{\sum (X_o - \overline{X_o})^2} \quad (1)$$

$$\mathrm{logNSE} = 1 - \frac{\sum (log(X_o) - \log(X_s))^2}{\sum (\log(X_o) - \log(\overline{X_o}))^2} \quad (2)$$

$$\mathrm{MB} = \frac{\sum X_s}{\sum X_o} - 1 \quad (3)$$

$$\mathrm{NRMSE} = \frac{\sqrt{\frac{1}{n}\sum (X_o - X_s)^2}}{\overline{X_o}} \quad (4)$$

where $X_s$, $X_o$ and $\overline{X_o}$ are the simulated, observed and mean of the observed hydrological variables, respectively, and $n$ is number of samples.

### 3.2. Model parameter estimation

GIS analyses of basin characteristics were conducted to derive basin physiographic, terrain visibility, and routing parameters for the HRUs in WGC basin. Parameter estimation for the key hydrological processes in the Boreal Hydrology Model of WGC basin is as follows.

Blowing snow parameters: vegetation heights were estimated from site observations; values of 7.6 m, 11 m, 8 m, 13 m, and 0.1 m were set for the HJP, OJP, ASP, OBS, Fen HRUs, respectively. For the blowing snow fetch distance, 300 m (minimum value) was used for all HRUs in the basin due to the short undisrupted upwind distance in the forest environment. This parameterisation effectively restricted blowing snow to the Fen HRU.

Canopy parameters: effective leaf area index (LAI) in winter for forest types were estimated as the mean values from the measurements in Chen et al. (1997) and Barr et al. (2012). Mean winter effective LAI values of 1.5, 2.4, 0.5, and 3.6 were assigned for the HJP, OJP, ASP, and OBS HRUs, respectively. A winter effective LAI of 0.1 was set for the open water and Fen HRUs given their low plant canopy coverage. The canopy snow interception capacity values were set based on similar forest types in studies of Schmidt and Gluns (1991), Hedstrom and Pomeroy (1998), and Pomeroy et al. (2002). Small values were set for the deciduous forest HRU as it does not have a high capacity to intercept and hold snow (Pomeroy and Gray, 1995). Therefore, a small canopy snow interception capacity of 0.5 kg/m$^2$ was assigned for the ASP HRU; higher values of 6.0 kg/m$^2$ and 5.9 kg/m$^2$ were set for OJP and OBS HRUs, respectively, while a lower value of 3.3 kg/m$^2$ was selected for the regenerated forest (i.e. HJP HRU) based on the process studies of Pomeroy and Granger (1997).

Soil moisture parameters: The model started on 1 October 1996, and value of 1.0 was set for initial soil saturation parameter, assuming the fall soil moisture is saturated after the rainy summer. The soil saturation was then updated based on soil moisture storage value every fall in the following hydrological years. Saturated hydraulic conductivities and pore size distributions for various soil layers were initialized based on the soil textures in WGC basin, and then slightly adjusted using trial and error based on the NSE and logNSE values of the streamflow simulation in the calibration period. The water storage capacities of soil layers were determined by multiplying soil layer depth by soil porosity. For the soil depth and porosity, averaged values for HRUs were estimated from the predominant soil texture in the basin (Agriculture and Agri-Food Canada, 2015). Groundwater storage capacity was relatively unknown, and so a maximum value of 200 mm was set for all HRUs. For surface depression storage capacities, values of 0.15–0.55 mm were set for all HRUs. The detention storage and runoff drainage factor which controls the rate of drainage from the organic layer were manually calibrated using trial and error based on the NSE and logNSE values of streamflow simulation in the calibration period of 1998–2007.

Routing parameters: the routing distribution parameter described by Fang et al. (2010) was used to model routing sequence between the six HRUs. The routing sequence generally follows the channel flow order from the upstream to the downstream part of the basin. Routing length of the main channel in each HRU was estimated from the terrain preprocessing GIS analysis. Manning's equation was used to calculate the average streamflow velocity based on longitudinal channel slope, Manning's roughness coefficient and hydraulic radius (Chow, 1964). The longitudinal channel slope was estimated as the Tangent of the average slope of the HRU. Manning's roughness coefficient was set to 0.016, considering the rather natural river channel in the basin. The hydraulic radius was assumed as 0.25 m for all HRUs. A value of 0.25 was assigned for the dimensionless weighting factor that controls the level of attenuation.

**Table 2**
Canopy parameters for HRUs in White Gull Creek basin.

| HRU name | Open water | Harvested jack pine (HJP) | Old jack pine (OJP) | Aspen | Old black spruce (OBS) | Fen |
|---|---|---|---|---|---|---|
| Area (km$^2$) | 16.4 | 33.4 | 67.2 | 137.3 | 254.1 | 94.2 |
| Elevation (m) | 520 | 536.5 | 557.3 | 563.6 | 568.6 | 570.1 |
| LAI | 0.1 | 1.5 | 2.4 | 0.5 | 3.6 | 0.1 |
| Vegetation height (m) | 0.001 | 7.6 | 11 | 8 | 13 | 0.1 |
| Snow interception capacity (kg/m$^2$) | 0 | 3.3 | 6 | 0.5 | 5.9 | 0 |

### 3.3. Perturbed precipitation and temperature inputs

Hourly observations of P and T in the period from 1 January 1998 to 31 December 2016 were used as reference climate inputs for the perturbed simulation. Linearly perturbed P and T time series were used to represent the possible ranges of climate until the end of the 21st century in the study basin.

Perturbed T inputs were set up by adding one-degree increments to the reference observed hourly air T, up to 6 ℃, as the maximum T increase in the study area is projected to about 6 ℃ until 2100 according to ECCC (2016) and the Canada's Changing Climate Report by Zhang et al. (2019). Perturbed P inputs were generated by multiplying the reference observed hourly P from 70% to 130%, because the maximum P change range in the study area is around ±30% until 2100 according to ECCC (2016) and the Canada's Changing Climate Report by Zhang et al.

(2019). Seasonality of P and T in the perturbed input time series were kept the same as that in the reference observations, as P and T in different months were perturbed by the same ranges. Relative humidity and wind speed were held same as those in the reference period. To focus on the hydrological sensitivity to climate perturbations, the forest disturbance caused by wildfire and human activity and changes in the soil properties such as reduced soil moisture storage from soil compaction during harvesting were not considered. Perturbed P and T inputs are summarized in Table 3. In total, six simulations of the perturbed T and six simulations of the perturbed P were conducted. Compensation between the effects of P and T perturbations on basin hydrology were investigated by combining each of the seven P simulations (six perturbed P and a reference P) with seven T simulations (six perturbed T and a reference T).

### 3.4. Quantifying the sensitivities of hydrological processes to perturbed climate inputs

The sensitivities of hydrological processes in the WGC basin were examined by changes in the selected magnitude and timing indices of water balance components or hydrological fluxes. Selected magnitude indices are annual runoff, seasonal runoff, annual peak runoff, annual peak SWE, annual snow sublimation, annual runoff coefficient, annual rainfall ratio, and annual evapotranspiration (ET); runoff components include groundwater flow, subsurface interflow from soil water, and snowmelt and rainfall overland flow. The investigated timing indices include timing of annual peak runoff, centre of mass timing (CMT) of annual runoff, timing of annual peak SWE, and duration of the snow-covered period. Sensitivities of magnitude indices (rm) were quantified in Eq. (5), in which $m_s$ refers to the magnitude index produced by the perturbed climate inputs and $m_r$ refers to the magnitude index forced by the reference climate inputs. Sensitivities of timing indices (rt) were estimated by differencing as in Eq.6. Similarly, $t_s$ refers to the timing index produced by the perturbed climate inputs and $t_r$ refers to the timing index forced by the reference climate inputs.

$$\mathrm{rm} = \frac{m_s - m_r}{m_r} \times 100\% \tag{5}$$

$$\mathrm{rt} = t_s - t_r \tag{6}$$

**Table 3**
Description of perturbed climate inputs in the White Gull Creek.

| Description | Precipitation input | Temperature input |
|---|---|---|
| Reference precipitation and temperature | Reference P | Reference T |
| Precipitation reduces by 30% | 70% of reference P | Reference T |
| Precipitation reduces by 20% | 80% of reference P | Reference T |
| Precipitation reduces by 10% | 90% of reference P | Reference T |
| Precipitation increases by 10% | 110% of reference P | Reference T |
| Precipitation increases by 20% | 120% of reference P | Reference T |
| Precipitation increases by 30% | 130% of reference P | Reference T |
| Temperature rises by 1 ℃ | Reference P | 1 ℃ higher than reference T |
| Temperature rises by 2 ℃ | Reference P | 2 ℃ higher than reference T |
| Temperature rises by 3 ℃ | Reference P | 3 ℃ higher than reference T |
| Temperature rises by 4 ℃ | Reference P | 4 ℃ higher than reference T |
| Temperature rises by 5 ℃ | Reference P | 5 ℃ higher than reference T |
| Temperature rises by 6 ℃ | Reference P | 6 ℃ higher than reference T |

## 4. Results

### 4.1. Model evaluation

Simulated SWE in the OJP and OBS HRUs were compared to site observations in Fig. 3. No calibration was performed for parameters that affect the forest and snow processes simulations. Over the entire study period (Fig. 3a-b), MB values were 0.1 and −0.15, and NRMSE values were 0.43 and 0.48 for simulated SWE at the OJP and OBS sites, respectively. These small MB and NRMSE values suggest that the model can adequately simulate snow accumulation and melt processes for mature jack pine and black spruce forests compared to the observations. The model generally captured the seasonal evolution of SWE in most years but had a large overestimation in two hydrological years: 2003–2004 and 2013–2014. While in the 2015–2016 hydrological year, the model underestimated the observed SWE. The relatively poor performance in these hydrological years is likely caused by the lack of accurate winter P measurements at both sites (similarly to Davison et al., 2016).

The model slightly overestimated annual ET at the OJP and OBS sites compared to the eddy correlation flux tower observations in the entire study period (Fig. 4). No calibration was done for parameters in the evapotranspiration simulation. MB value for simulated annual ET at OJP was 0.11, while MB for simulated annual ET at OBS was only 0.03. This suggests that the overestimation is within 11% at both sites, and the model could adequately obtain the annual ET flux value for most years except for 2004–2006 and 2013–2014 when model estimated large differences in annual ET compared to observations at the two forest sites.

Modelled soil volumetric water content (VWC) in the OJP and OBS HRUs were compared with observations in Fig. 5. No calibration was performed for parameters to fit the soil moisture observation, and comparisons were only conducted for unfrozen months (1 May to 30 September). For observed VWC, the weighted average of soil VWC of the layers of 0–15 cm and 15–30 cm was used to represent the VWC for the upper layer (0–28 cm), and the weighted average of layers of 15–30 cm and 30–60 cm was used as VWC of the lower layer (28–45 cm). For both modelled and observed soil VWC, values at the OJP site were lower than those at the OBS site, as soil type is mainly loam sand at the OJP site and typically clay at the OBS site. At the OJP site (Fig. 5a-b), the model generally overestimated VWC, with MB values ranging from 0.11 for lower layer to 0.12 for upper layer. NRMSE values were no higher than 0.3, indicating reasonable model performance for seasonal soil moisture estimation at this site. At the OBS site (Fig. 5c-d), the model underestimated VWC of the upper layer with MB values of −0.13; for the lower layer, the model overestimated by 2% (i.e. MB = 0.02). The NRMSE values were within 0.26 in both soil layers, suggesting model adequately captured the seasonal fluctuations of soil moisture at the OBS site.

Fig. 6 shows the comparisons of simulated and observed daily mean streamflow in WGC basin in two periods, one for a parameter calibration period (1998–2007) and one for a validation period (2008–2016). Observed streamflow in the year of 2011 was discarded for the evaluation, considering the measurement errors noted in this year (Davison et al., 2016). The model achieved logNSE values of 0.8 and 0.74 in calibration and validation periods, respectively, indicating that model could simulate the low flows well in winter months. NSE values were 0.63 and 0.6 in the calibration and validation periods, respectively, suggesting that model's capability to predict high flows in spring and summer months was adequate but not as good as that for winter low flows. MB values show that the model captured streamflow volume well in the WGC basin, with 4% overestimation and 12% underestimation in the calibration and validation periods, respectively. Considering the sparse observations of meteorological data, uncertainty in streamflow estimates, and the complex land cover condition in the basin, the model generally obtains reasonable streamflow simulations and is comparable to results from the MESH hydrological land surface model previously

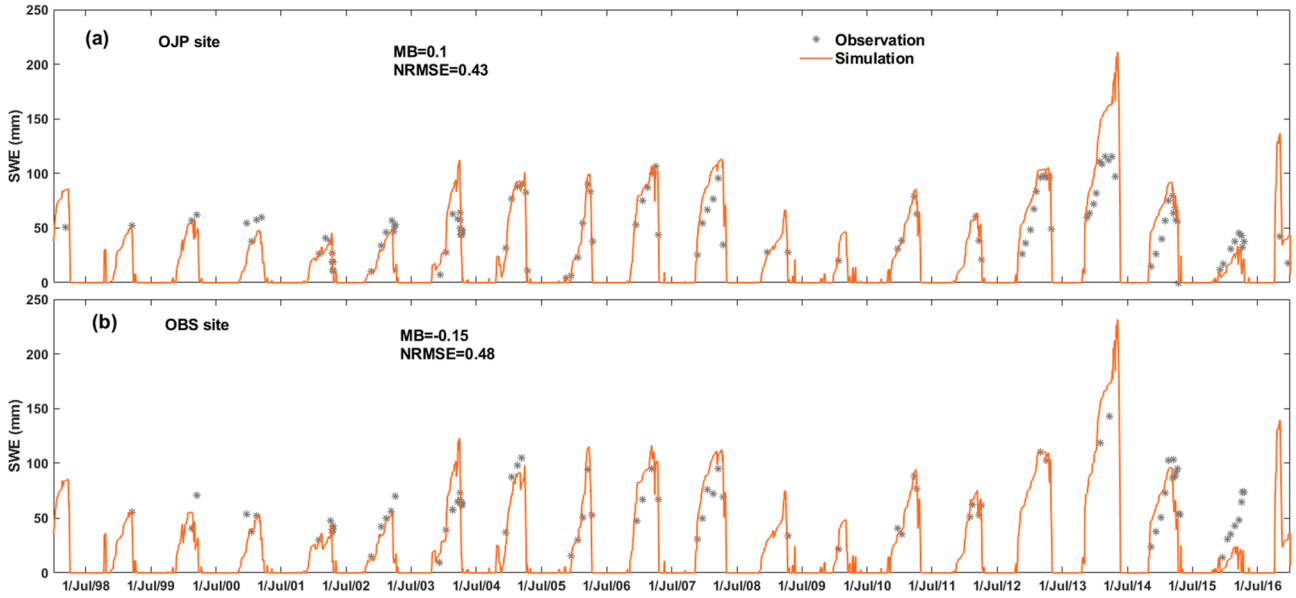


**Fig. 3.** Comparisons of simulated and observed SWE at the OJP and OBS sites in the modeling period of 1998–2016.

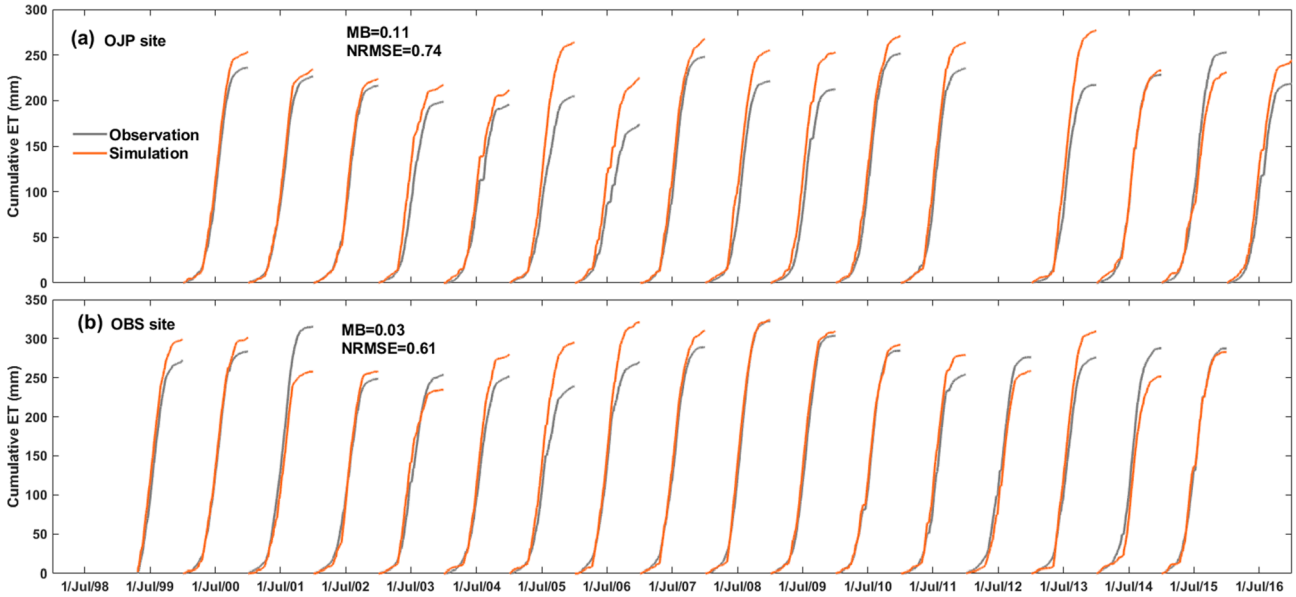


**Fig. 4.** Comparisons of simulated and observed cumulative ET at the OJP and OBS sites in the modeling period of 1998–2016. The cumulative ET was calculated for a water year from January 1st to December 31st.

applied to this basin in Davison et al. (2016).

### 4.2. *Sensitivities of hydrological variables to perturbed P and T*

Sensitivities of the selected magnitude and timing indices of hydrological variables to perturbed P and T are compared in Fig. 7 and Table 4. Annual runoff and maximum daily runoff responded directly to changing P and inversely with warming T, however sensitivities varied markedly (Fig. 7a). For a decrease in P of 30% from the current climate, the annual runoff and maximum runoff decreased by 61% and 52%, respectively, whereas they rose by 93% and 108% as the P increased by 30% (Table 4). With 6 ℃ of warming, the annual runoff and maximum runoff declined by 23% and 35%, respectively (Fig. 7a). The centre of mass timing (CMT) of annual runoff varied directly with changing precipitation (Fig. 7b), in which it advanced by 17, 9, and 4 days in response to decreases in P of 30%, 20%, and 10%, respectively, and recessed by 4, 8, and 10 days when P increased by 10%, 20%, and 30%, respectively (Table 4). It responded to warming T in a near linear but inverse manner (Fig. 7b) and advanced by 19 days for 6 ℃ of warming. However, the timing of maximum runoff responded non-linearly to P and T perturbations (Fig. 7b). There was little sensitivity of the maximum runoff timing to perturbed P except for increases in P of 20%-30% for which the maximum runoff timing recessed sharply by up to 32 days (Table 4). This suggests threshold behaviour in runoff timing in the basin. The annual maximum runoff occurred earlier with warming T but with substantial variability, where 5 ℃ of warming resulted in an advance of 22 days, but 6 ℃ of warming advanced the maximum runoff timing by only 14 days.

The volume of annual peak SWE varied almost linearly with P (Fig. 7c), declining by 36%, 24%, and 12% as P declined by 30%, 20%, and 10%, and increasing by 12%, 24%, and 37% as P increased by 10%, 20%, and 30% (Table 4). Peak SWE declined by 13% as T increased by

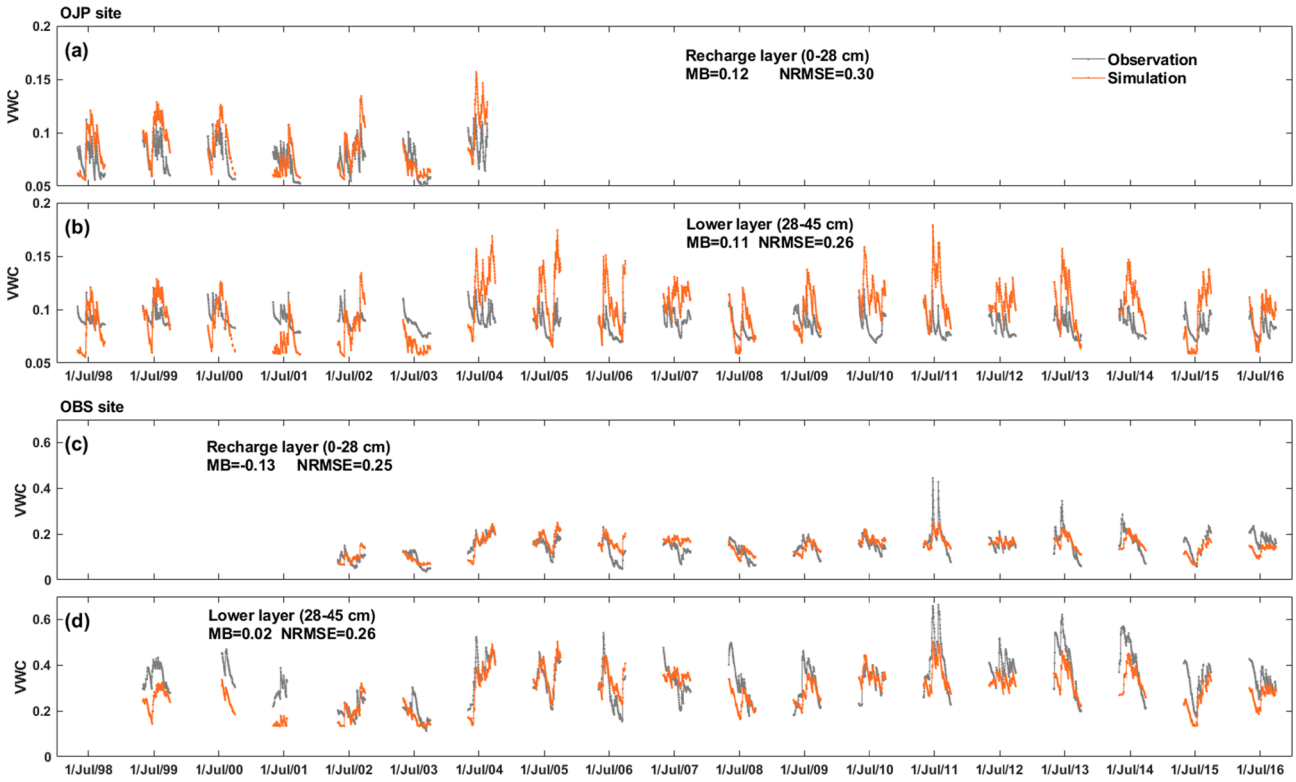


**Fig. 5.** Comparisons of simulated and observed soil liquid volumetric water content (VWC) at the OJP and OBS sites. Comparisons were only done when VWC measurements were available.

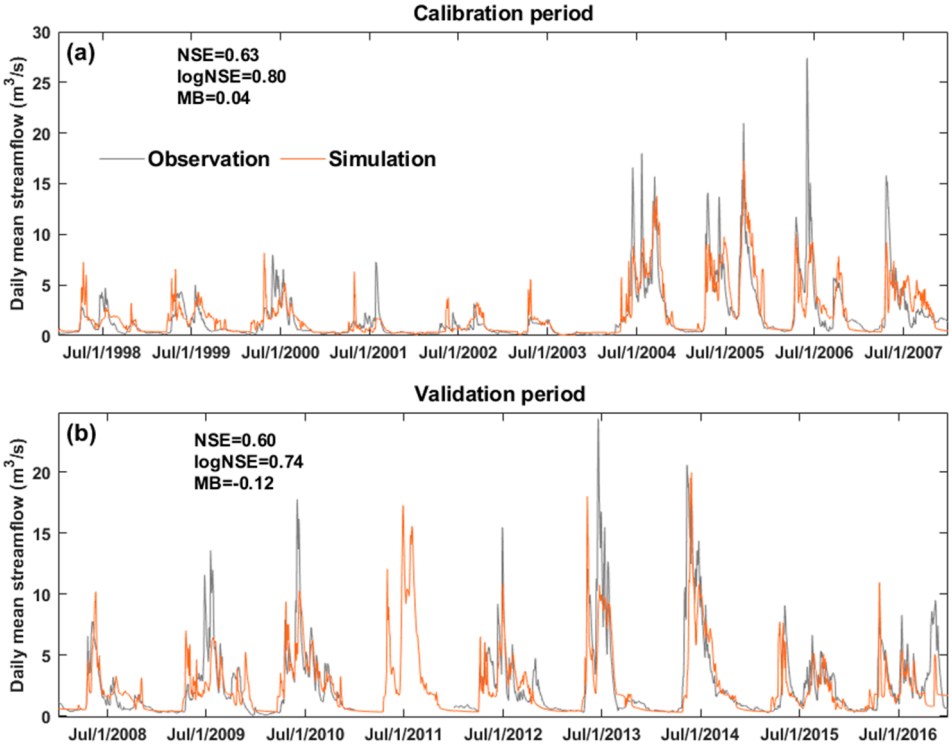


**Fig. 6.** Comparisons of simulated and observed daily mean streamflow in White Gull Creek in (a) calibration (1998–2007) and (b) validation (2008–2016) periods.

1 °C and by 61% for an increase of 6 °C above reference levels (Fig. 7c, Table 4). Annual ET was insensitive to perturbed P, increasing very slightly, by 3%, for a P increase of 30% and declining by only 8% for a P decrease of 30%. In contrast, ET was very sensitive to warming with a 42% increase for 6 °C of warming (Fig. 7c and Table 4). The timing of annual peak SWE and the snow-cover duration also responded more strongly to perturbed T than to perturbed P (Fig. 7d). When P increased by 30%, the date of annual peak SWE recessed by 4 days and the snow-

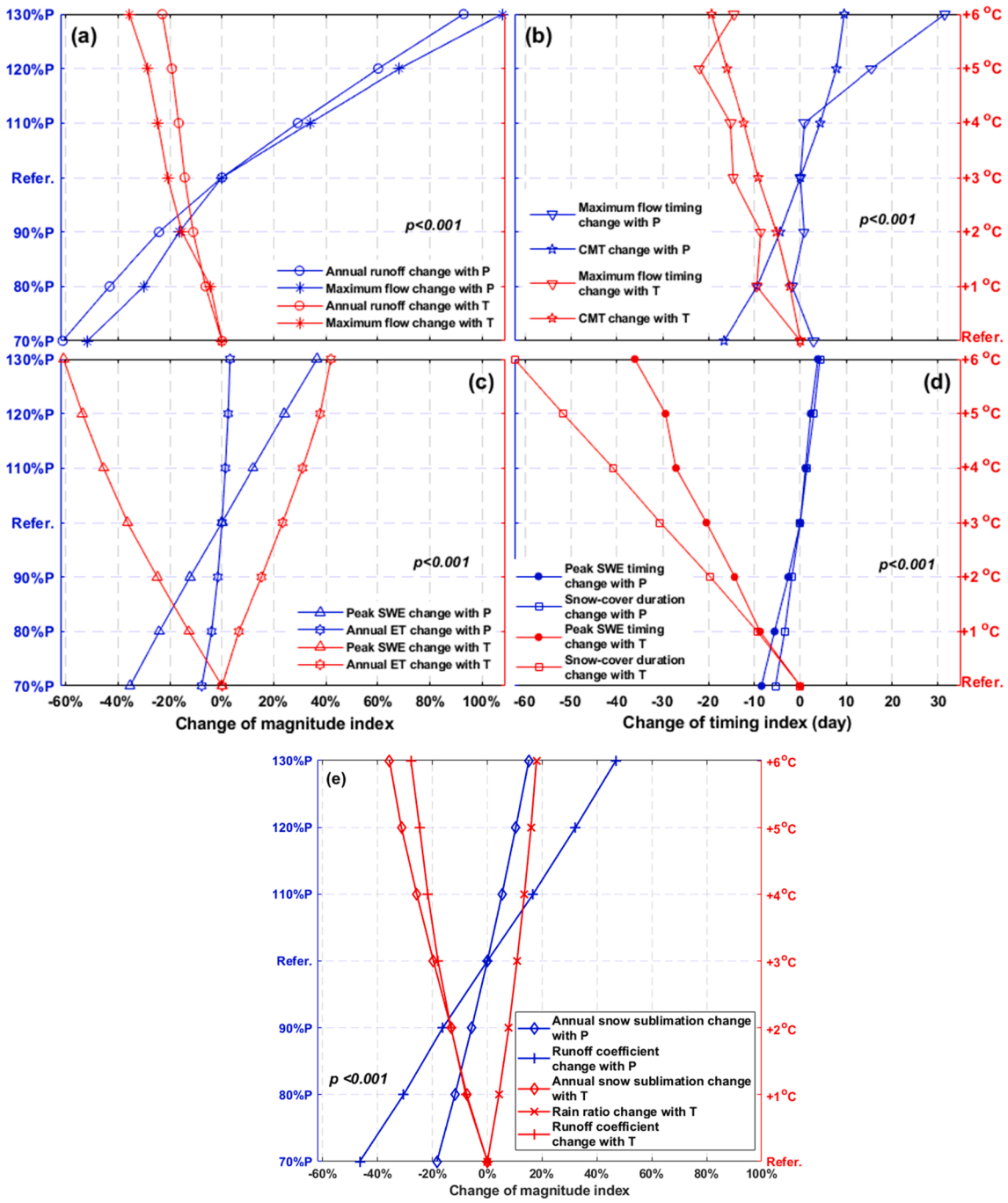


**Fig. 7.** Sensitivities of the selected magnitude and timing indices of hydrological variables to perturbed precipitation (blue lines) and temperature (red lines). (a) annual runoff and maximum flow, (b) timing of maximum flow and centre mass timing (CMT) of annual runoff, (c) annual peak SWE and annual ET, (d) timing of annual peak SWE and snow-cover duration, and (e) annual snow sublimation, rain ratio of annual precipitation, and runoff coefficient. *p* values show the significant level for all the variable change trends with climate perturbations.

cover duration increased by 4 days; whilst the date of annual peak SWE advanced by 9 days and the snow-cover duration shortened by 9 days for just 1 ℃ of warming. Remarkably, 6 ℃ of warming resulted in a 36-day advance in the timing of peak SWE and a 62-day decline in snow-cover duration (Table 4).

Fig. 7e compares the sensitivities of annual snow sublimation, runoff coefficient and rainfall ratio to the perturbed P and T. Annual snow sublimation increased by 15% as the annual P rose by 30%, whilst it decreased by around 18% with a P reduction of 30%. The impact of warming T on annual snow sublimation is very high; a 7% reduction in snow sublimation was caused by 1 ℃ of warming and a 36% decrease corresponded to 6 ℃ of warming. The runoff coefficient was enhanced near linearly with increases in P at an average rate of 16% per 10% increase in P; whilst reductions in the runoff coefficient were at an average rate of 4.7% per 1 ℃ of warming due to the enhanced annual ET (Fig. 7c). Rainfall ratio was insensitive to perturbed P but increased at an average rate of 3% per 1 ℃ of warming.

### 4.3. Changes of streamflow regime in response to P and T perturbations

The simulated monthly runoff forced by reference P in 1998–2016, and 30% increase and decrease in P are compared to illustrate the intra-

**Table 4**
Sensitivities of hydrological variables to perturbed precipitation (P) and air temperature (T). Mean changing rate was calculated by dividing the largest variables changes with the largest perturbations of P (3*±10%) and T (+6 ℃).

| P inputs | 70% P | 80% P | 90% P | Refer. P | 110% P | 120% P | 130% P | Mean changing rate |
|---|---|---|---|---|---|---|---|---|
| Annual runoff | −61% | −44% | −24% | 0% | 29% | 60% | 93% | +31%/+10%P; −20%/-10%P |
| Annual maximum runoff | −52% | −30% | −16% | 0% | 34% | 68% | 108% | +36%/+10%P; −17%/-10%P |
| Peak SWE | −36% | −24% | −12% | 0% | 12% | 24% | 37% | +12%/+10%P; −12%/-10%P |
| Annual ET | −8% | −4% | −2% | 0% | 1% | 2% | 3% | +1%/+10%P; −3%/-10%P |
| Annual snow sublimation | −18% | −12% | −6% | 0% | 5% | 10% | 15% | +5%/+10%P; −6%/-10%P |
| Runoff coefficient (R/P) | −46% | −31% | −16% | 0% | 17% | 32% | 47% | +16%/+10%P; −15%/-10%P |
| Maximum runoff timing (day) | 3 | −2 | 1 | 0 | 1 | 16 | 32 | +11 day/+10%P; +1day/-10%P |
| Centre of mass timing (CMT, day) | −17 | −9 | −4 | 0 | 4 | 8 | 10 | +3day/+10%P; −6day/-10%P |
| Peak SWE timing (day) | −8 | −6 | −3 | 0 | 1 | 2 | 4 | +1day/+10%P; −3day/-10%P |
| snow-cover duration (day) | −5 | −3 | −2 | 0 | 1 | 3 | 4 | +1day/+10%P; −2day/-10%P |
| T inputs | Refer. T | T +1 ℃ | T +2 ℃ | T +3 ℃ | T +4 ℃ | T +5 ℃ | T +6 ℃ | Mean changing rate |
| Annual runoff | 0% | −6% | −11% | −14% | −17%% | −19% | −23% | −3.8%/+1 ℃ |
| Annual maximum runoff | 0% | −4% | −15% | −21% | −24% | −28% | −35% | −5.8%/+1 ℃ |
| Peak SWE | 0% | −13% | −25% | −36% | −45% | −54% | −61% | −10%/+1 ℃ |
| Annual ET | 0% | 7% | 15% | 23% | 31% | 38% | 42% | +7%/+1 ℃ |
| Annual snow sublimation | 0% | −7% | −13% | −20% | −26% | −31% | −36% | −6%/+1 ℃ |
| Runoff coefficient (R/P) | 0% | −8% | −13% | −18% | −22% | −25% | −28% | −4.7%/+1 ℃ |
| Rain ratio (Rain/P) | 0% | 4% | 8% | 11% | 13% | 16% | 18% | +3%/+1 ℃ |
| Maximum runoff timing (day) | 0 | −9 | −8 | −14 | −15 | −22 | −14 | −2.3 day/+1 ℃ |
| Centre of mass timing (CMT, day) | 0 | −2 | −5 | −9 | −12 | −16 | −19 | −3.2 day/+1 ℃ |
| Peak SWE timing (day) | 0 | −9 | −14 | −21 | −27 | −29 | −36 | −6day/+1 ℃ |
| snow-cover duration (day) | 0 | −9 | −20 | −31 | −41 | −52 | −62 | −10 day/+1 ℃ |

annual variability of basin runoff for varied levels of P input (Fig. 8a). Lower P resulted in a smaller runoff volume that is distributed more evenly over the seasons in contrast to increasing P that leads to substantially larger runoff volumes being generated in warm months (May to September) and much greater runoff for low frequency events on the flow duration curve (FDC) calculated over the entire simulation period (Fig. 8c). The simulated monthly runoff from the reference T, and warming of 1 ℃ and 6 ℃ are compared in Fig. 8b. Increasing T resulted in a more even distribution of monthly runoff; with T increasing by 6 ℃, the runoff in April to September was reduced, leading to reduced runoff for low frequency events as evident by changes to the FDC (Fig. 8d). The variations of monthly runoff in the boxplots (Fig. 8a and 8b) were estimated from the monthly runoff in each year of the entire study period, indicating the inter-annual variability of monthly runoff during the simulation period. Increasing P enhanced the inter-annual variability of runoff, especially for the warm months, whilst raising T reduced the inter-annual variability of runoff in the warm months but increased the inter-annual variability of runoff in the cold months. The higher variability of runoff in the cold months with warming T is due to increasing mid-winter melt events and likely complex interactions with frozen soils and basal ice layers, and the lower variability of runoff in warm months with warming T is result of lower antecedent soil moisture impact on rainfall-runoff generation. The inter-annual variability of simulated daily hydrographs from the above perturbed P and T are illustrated in Fig. 8e-f. Again, the inter-annual variability of daily runoff in warm months increased with P but decreased with T.

Sensitivities of seasonal runoff and runoff components to P and T perturbations in WGC basin are shown in Fig. 9 and Table 5. The seasonal runoff generally increased with P (Fig. 9a), but the relative contributions of spring (MAM, March to May) and winter (DJF, December to February) runoff to annual volumes declined as P increased (Fig. 9c). When P increased from 70% to 130% of the reference observation, the winter and spring runoff increased by 4 mm and 45 mm (Table 5), whilst their contributions to the annual runoff volume decreased by 9% and 5%, respectively (Fig. 9c). For the same P increase, autumn (SON, September to November) runoff increased by about 40 mm, with little change in its contribution to the annual runoff; summer (JJA, June to August) runoff rose by about 91 mm, with its contribution to annual runoff increasing by 14% (Fig. 9c), partly because of the enhanced rainfall storms in summer. In contrast, seasonal runoff volumes generally decreased with rising T, except for winter runoff (Fig. 9b). The fractional contribution of summer runoff decreased by 11% as T rose by 6 ℃ (Fig. 9d). Such T rise promoted increasing fractions of runoff generation in cold seasons, resulting in 5.7% and 4.6% higher contributions for autumn and winter runoff, respectively, but little change in the fractional contributions from spring runoff.

Sensitivities of the major runoff components: deep groundwater flow, subsurface interflow from soil water, snowmelt overland flow and rainfall overland flow to the P and T perturbations are shown in Fig. 9a-b and e-f. Both P and T increases led to a higher contribution of subsurface interflow to total runoff and little change in the contribution of rainfall overland flow to total runoff (Fig. 9e-f). Groundwater flow generally increased with higher P and rose by about 70 mm when P increased from 70% to 130% of the reference observations (Table 5), but its contribution to total runoff diminished because there was much higher increase of 179 mm in total runoff, dominated by an increase in subsurface interflow. While groundwater flow decreased with warming T, its fractional contribution to total runoff remained unchanged (Fig. 9f). Snowmelt overland flow increased with higher P and declined with warmer T (Table 5), yet its fractional contribution to total runoff decreased when either P or T increased (Fig. 9e-f). Overall, the contributions of runoff components tended to show higher sensitivities to P perturbation than to T perturbation.

### 4.4. Compensatory effects of P and T perturbations

As shown in Fig. 7, increasing P resulted in higher annual runoff, while warming T reduced the generation of runoff. The compensatory effects of P and T perturbations on hydrological processes were therefore explored. Fig. 10 shows strong sensitivities of annual runoff to changing precipitation, snow-covered duration to T, and peak SWE date, CMT of annual runoff, runoff coefficient and snow sublimation to both T and P. Reduction of annual runoff caused by 1 ℃ of warming could be compensated for by the runoff increase from a 1.7% increase in P (Fig. 10a), and the advance of the annual runoff CMT caused by 1 ℃ of warming could be compensated for by a 7% P increase (Fig. 10b). The reduction of annual runoff caused by 6 ℃ of warming could be compensated for by runoff increase generated by a 10% increase in precipitation. However, the maximum increase in P considered (+30%) could only compensate for the advance in CMT of annual runoff caused by 3.8 ℃ of warming. The reduced magnitude of runoff coefficient caused by 1 ℃ of warming could be compensated for when a 4.5%

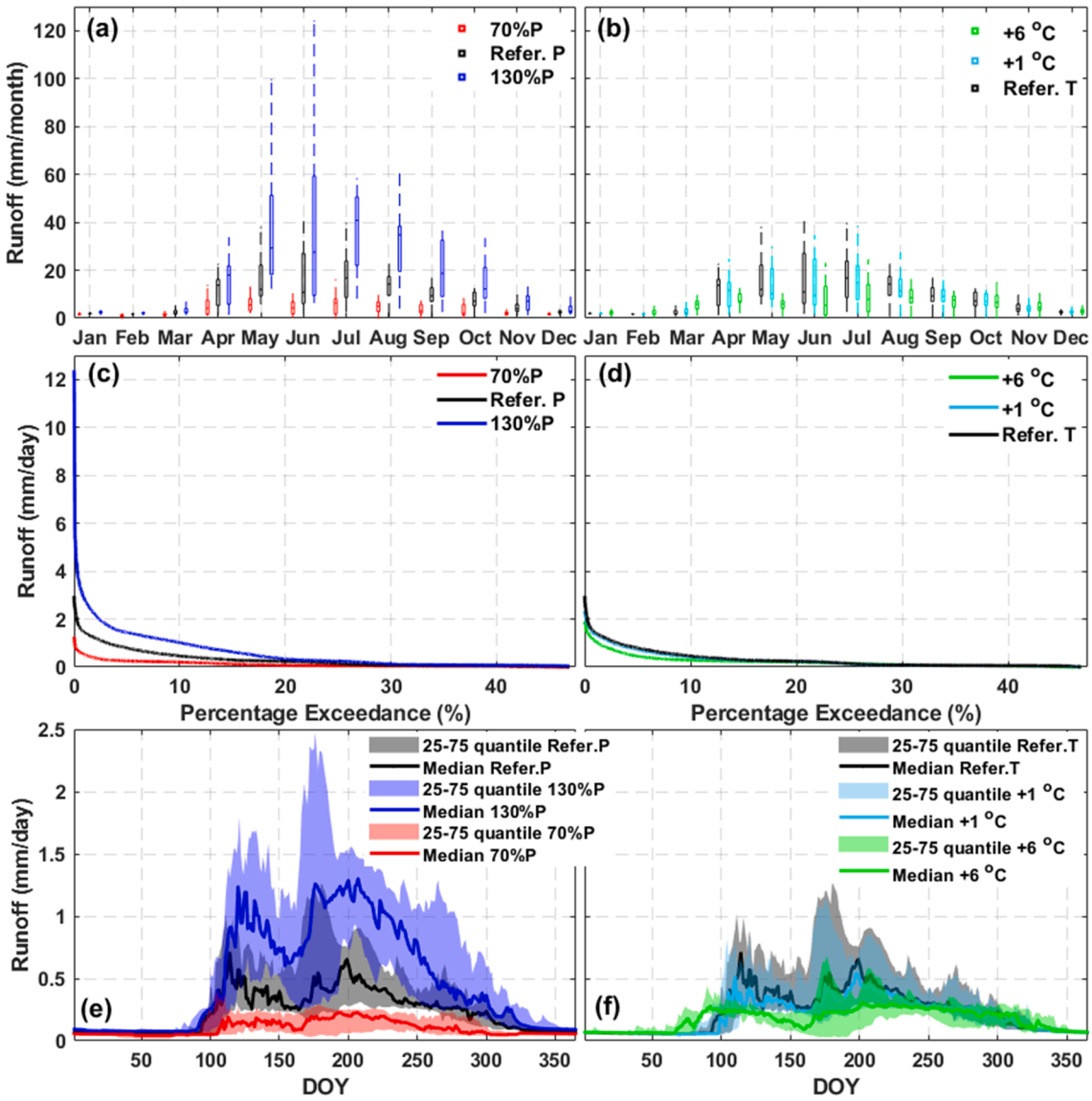


**Fig. 8.** Sensitivities of the intra- and inter-annual variabilities of runoff to perturbed precipitation and temperature in the simulation period of 1998-2016. (a)-(b) monthly runoff, (c)-(d) flow duration curve (FDC), and (e)-(f) daily runoff.

increase in P occurred (Fig. 10c). A 19% increase in P could completely compensate for the reduction of runoff coefficient caused by the highest warming of 6 ℃. Decreases in peak SWE and annual snow sublimation caused by 1 ℃ of warming could be compensated for by 13% and 15% increases in P, respectively (Fig. 10d and f), but the maximum increase of P (+30%) could only compensate for the reductions in peak SWE and snow sublimation caused by 2.2 ℃ and 2 of ℃ warming, respectively. Decrease in snow-cover duration caused by 1℃ of warming could not be compensated for (Fig. 10e), even by the upper bound of 30% increase in precipitation.

Fig. 11a-d show that subsurface interflow and rainfall overland flow are most sensitive to P, whilst groundwater flow and snowmelt overland flow are sensitive to both P and T. Compensatory behaviour by P and T in controlling the sensitivities of runoff components follows those relationships. Reduction of groundwater from 1 ℃ of warming could be compensated for by a 3% P increase, while decreased subsurface interflow and snowmelt overland flow caused by 1 ℃ of warming were offset by 1% and 7% P increases, respectively. Reduction of groundwater and subsurface interflow caused by the maximum warming of 6 ℃ could be offset by 18% and 5% P increases, respectively. However, the maximum increase in P (+30%) could only compensate for reduction of snowmelt overland flow caused by around 4 ℃ of warming and there was no consistent compensatory behaviour by P and T for the sensitivity of rainfall overland flow (Fig. 11d).

Fig. 11e-h shows that spring and autumn runoff are strongly affected by increases in P and less affected by rises in T, whilst winter runoff is more sensitive to warming T for the higher P (i.e. 110% to 130% P perturbations). The reduction of spring runoff caused by 1 ℃ of warming could be compensated for by a 4% P increase, whilst decreased summer runoff and autumn runoff caused by 1 ℃ of warming were offset by 3% and 0.7% increases in P, respectively. The reductions of runoff in spring, summer, and autumn caused by the maximum T warming (+6 ℃) could be compensated for by P increases of about 16%, 18% and 4%, respectively. Increasing P and rising T both tended to result in higher winter runoff, and thus the maximum warming of + 6 ℃ could offset the loss in winter runoff caused by a 12% decrease in P.

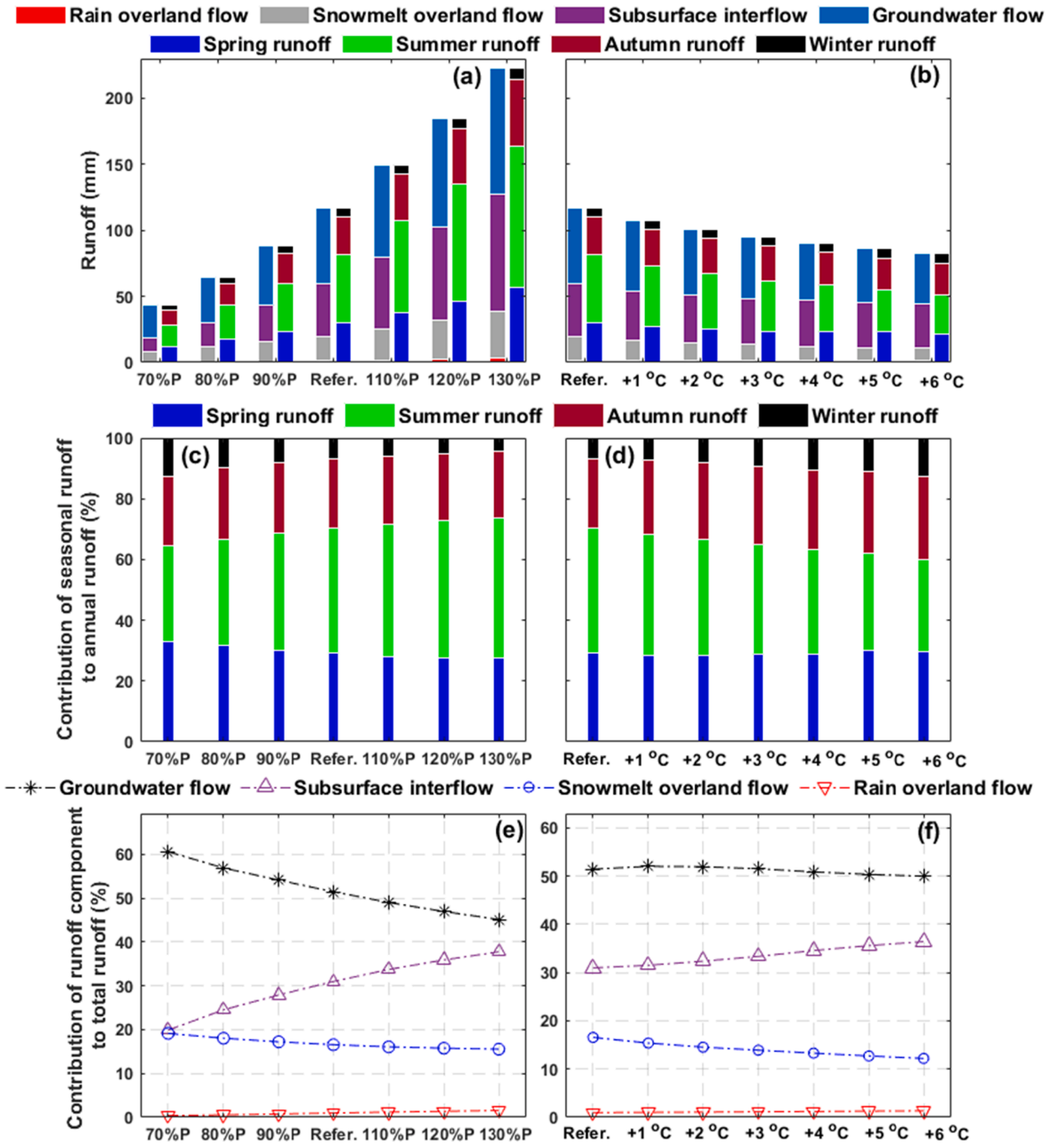


**Fig. 9.** Sensitivities of seasonal runoff and runoff components to perturbations of P and T. (a)-(b) amounts of seasonal runoff and runoff components, (c)-(d) contributions of seasonal runoff to annual runoff, and (e)-(f) contributions of runoff components to the total runoff.

## 5. Discussion

### *5.1. Variable sensitivities of runoff and snow processes to P and T perturbations*

In White Gull Creek (WGC) basin, the non-linear sensitivity of hydrological variables to perturbed P could be partly attributed to the complex effects of soil storage. In particular, P had primary control on the water availability and its variation affected the runoff generation in WGC (Davison et al., 2016). Under low P input conditions, P mainly supported infiltration into soils to fill the soil and groundwater storages and was exhausted by ET loss back to atmosphere, leading to lower runoff. In contrast, higher P more likely saturated the soil and groundwater storages and promoted greater runoff generation. As a result, the annual runoff and peak runoff showed larger sensitivity to the changes of P under high P input conditions (Table 4 and Fig. 7a). Subsurface interflow and groundwater flow were more sensitive to perturbed P compared to rainfall and snowmelt overland flows (Fig. 9a and Table 5), as P primarily infiltrated into the porous forest soils in WGC. On the other hand, the basin peak SWE showed linear sensitivity to perturbed P, as soil storage has no effect on the snow accumulation. The sensitivities of runoff and snow processes to P perturbation are generally consistent with those findings in other cold regions (such as López-Moreno et al., 2012; Rasouli et al., 2014).

The non-linear sensitivities of runoff processes to perturbed T can be partly explained by the effects of warming on ET, snow cover

**Table 5**
Amounts (mm) for seasonal runoff and runoff components simulated by multiple combinations of precipitation and temperature inputs.

| Using Refer. T | 70% P | 80% P | 90% P | Refer. P | 110% P | 120% P | 130% P |
|---|---|---|---|---|---|---|---|
| Spring runoff (MAM) | 12 | 18 | 23 | 30 | 38 | 46 | 57 |
| Summer runoff (JJA) | 16 | 25 | 37 | 51 | 69 | 89 | 107 |
| Autumn runoff (SON) | 11 | 17 | 23 | 29 | 36 | 43 | 51 |
| Winter runoff (DJF) | 4 | 5 | 6 | 6 | 7 | 8 | 8 |
| **Total annual runoff** | **44** | **65** | **88** | **117** | **150** | **185** | **223** |
| | | | | | | | |
| Rain overland flow | 0.2 | 0.4 | 0.7 | 1.1 | 1.7 | 2.5 | 3.4 |
| Snowmelt overland flow | 8. | 11 | 15 | 19 | 24 | 29 | 35 |
| Subsurface interflow | 10 | 18 | 28 | 40 | 55 | 71 | 89 |
| Groundwater flow | 25 | 35 | 45 | 57 | 70 | 82 | 95 |
| **Total annual runoff** | **44** | **65** | **88** | **117** | **150** | **185** | **223** |
| | | | | | | | |
| Using Refer. P | Refer. T | +1 ℃ | +2 ℃ | +3 ℃ | +4 ℃ | +5 ℃ | +6 ℃ |
| Spring runoff (MAM) | 30 | 27 | 25 | 24 | 23 | 23 | 22 |
| Summer runoff (JJA) | 51 | 46 | 43 | 39 | 35 | 32 | 29 |
| Autumn runoff (SON) | 29 | 28 | 27 | 26 | 25 | 24 | 24 |
| Winter runoff (DJF) | 6 | 6 | 6 | 6 | 7 | 7 | 8 |
| **Total annual runoff** | **117** | **107** | **100** | **95** | **90** | **86** | **83** |
| | | | | | | | |
| Rain overland flow | 1.1 | 1.0 | 1.0 | 1.0 | 1.0 | 1.0 | 1.0 |
| Snowmelt overland flow | 19 | 16 | 14 | 13 | 11 | 10 | 10 |
| Subsurface interflow | 40 | 38 | 36 | 35 | 35 | 34 | 34 |
| Groundwater flow | 57 | 53 | 49 | 46 | 43 | 41 | 38 |
| **Total annual runoff** | **117** | **107** | **100** | **95** | **90** | **86** | **83** |

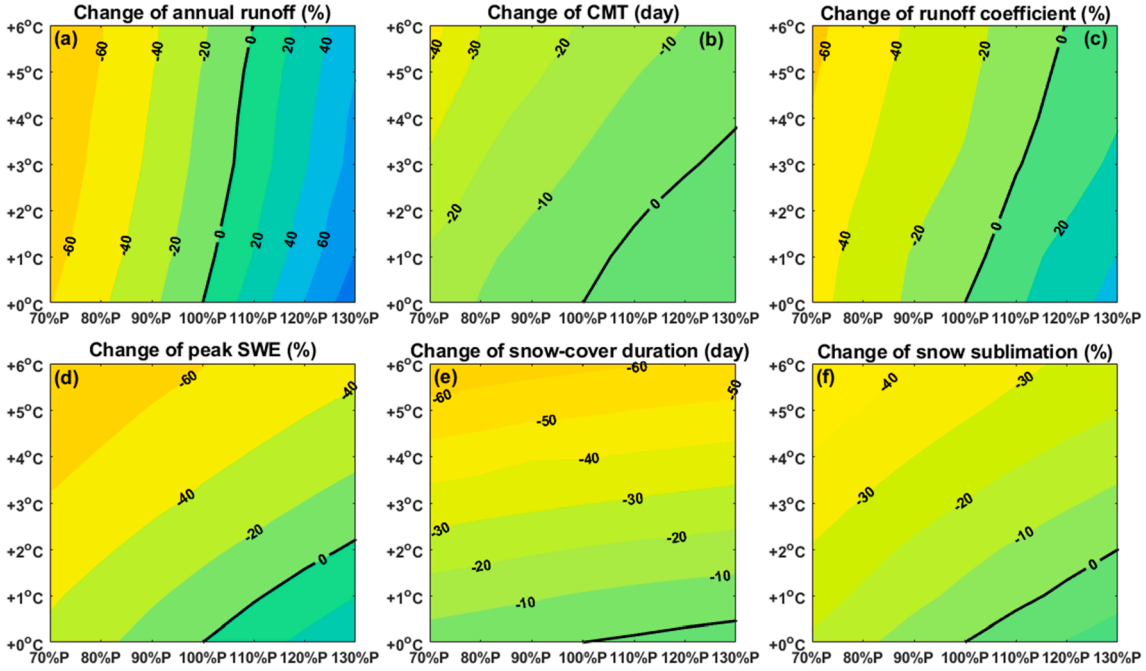


**Fig. 10.** Sensitivities of annual runoff, centre of mass timing (CMT), runoff coefficient, peak SWE, snow-cover duration, and annual snow sublimation to combined perturbations of P and T. Note that compensation contour indicates the effect caused by warming temperature was compensated for by the increased precipitation and is labeled with value 0.

disappearance and the thawing of frozen soil. In particular, warming leads to higher ET and increases the infiltration capacity of frozen soil in this basin (Ireson et al., 2015). For fixed P input, the increased ET due to warming has an important control on the annual volume of runoff from WGC (Nijssen and Lettenmaier, 2002). The complicated ET increases in response to warming shown in Fig. 7c are results of complex processes in soil moisture, transpiration season and rainfall interception that both affect annual ET losses, and this non-linear sensitivity of ET to perturbed T is consistent with the findings in boreal forest by Brown et al. (2014). On the other hand, warming T accelerates the thawing of frozen soil (Endalamaw et al., 2017) and promotes the contribution of subsurface interflow to the total runoff. In addition, the psychrometric energy balance method used for P phase partitioning (Harder and Pomeroy, 2013) and complex snow processes such as sublimation and interception in boreal forest (Hedstrom and Pomeroy, 1998) as well as energy-balance based snowmelt estimation (Marks et al., 1998) are sensitive to T and could be reasons for the non-linear response of peak SWE to T perturbation. These non-linear effects of warming on hydrological and snow processes in WGC are generally similar to the findings demonstrated by Woo et al. (2008) and Holmberg et al. (2014) in other boreal forests.

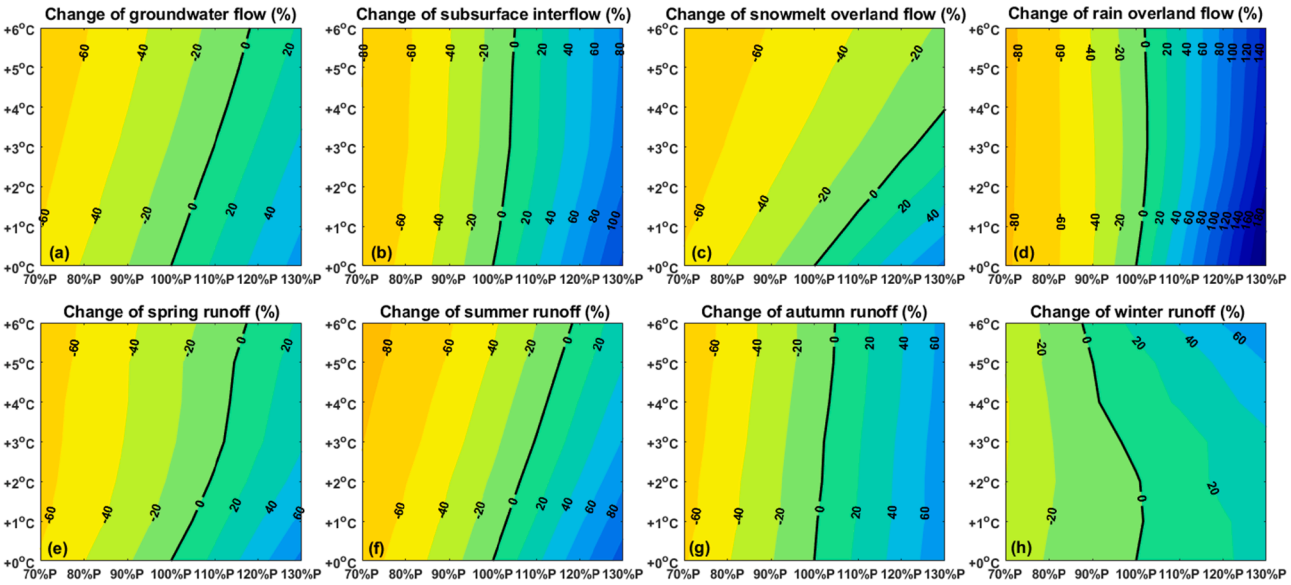


**Fig. 11.** Sensitivities of runoff components and seasonal runoff to combined perturbations of P and T, noting compensatory effects of precipitation and temperature changes are labeled with value 0 on contour.

### *5.2. Limitations*

The effects of climate on forest canopy, such as the increasing wildfire occurrence and intensity, as well as the gradual reduction in canopy LAI and snow interception capacity caused by T warming and drought (Boulanger et al., 2016) were not considered. The disturbance of forest by potential wildfire or disease and the regrowth of harvested forest as well as the change of soil properties in the basin were also not considered in this study when investigating the sensitivities of hydrological processes to P and T perturbations. This investigation procedure is similar to the hydrological sensitivity analysis to perturbed climate by Rasouli et al. (2014) and Rasouli et al. (2015).

This study focuses on the sensitivity of hydrological processes to perturbed P and T, instead of projection of future hydrology using an ensemble forcing data from Earth System Models (ESMs). The linear perturbations of precipitation and temperature are not climate change scenarios projected by ESMs, but rather provide a range of potential future changes. This climate perturbation method was used because of its special function on investigating what combinations of precipitation and temperature changes can induce significant hydrological changes in the boreal forest basin (Rasouli et al., 2014) and what the roles of particular P or T perturbations are in shaping the responses of specific hydrological processes. This simple method avoided the heavy computational cost of dynamically downscaling climate models to the size of the study basin (~600 km$^2$), and provided climate inputs with reasonable spatial and temporal patterns with observed extremes such as dry, cold, warm and storm (Rasouli et al., 2019). This sensitivity analysis serves as an early step to understand the shifts of boreal forest hydrology under a wide range of P and T perturbations. One limitation of the linearly perturbed P and T inputs falls in that the seasonal patterns of P and T in the perturbed scenarios are kept same as that in the reference observations. More extensive analysis to include the changes in seasonal P and T, as well as the changes in rain and snow characteristics such as intensity and frequency could be helpful to provide more informative sensitivity estimation of hydrological process in the basin (Rasouli et al., 2014). Despite that, the current simple method has informed the vulnerability of boreal forest hydrology to the changes in P and T and quantitatively revealed that the impacts of warming on hydrological processes depend strongly on P changes.

Uncertainty in the hydrological modelling forms another limitation. The selection of model parameter values has large effects on the estimated sensitivities of hydrological processes to climate perturbations. In this study, snow process, soil and canopy parameter values were estimated based on field measurements and knowledge gained from fieldwork. Previous applications of CRHM-created models in the cold regions of Canada indicate that setting these parameters based on understandings of the study basins from field research (Ellis et al., 2010, Fang et al., 2013), and calibrating a small group of parameters such as soil hydraulic and storage by observed streamflow (Krogh et al., 2017) had the potential to identify plausible values for the model parameters. Uncertainty of the model structure, such as the insufficient representation for the poorly drained wetlands, could lead to the underestimations of peak flow in summer (Davison et al., 2016). To improve the representation for wetlands, an alternative is to refine the HRUs in the model. However, complex routing sequences among HRUs when including more wetland HRUs can potentially pose additional uncertainty for hydrological modelling in WGC.

## 6. Conclusions

This study investigated the sensitivities of runoff and snow processes to perturbed climate in a well instrumented boreal forest basin White Gull Creek (WGC) in Western Canada. A Boreal Hydrology Model of the key hydrological processes and basin streamflow response was set up using the CRHM platform and was parameterised primarily from knowledge of the basin with minor calibration using streamflow simulations for parameters describing drainage of the soil organic layer. The model was verified against measurements of snow accumulation, soil moisture and streamflow, and eddy correlation flux tower observations of evapotranspiration (ET), and was found to represent the hydrological cycle of the boreal forest reasonably well. Sensitivities of modelled hydrological processes to perturbed climate were quantified using perturbations of observed time series of precipitation (P) and air temperature (T). The major findings are:

(1) The basin hydrological variables presented variable sensitivities to perturbations of P and T. Annual runoff volume and maximum daily streamflow increased rapidly with rising P at rates of around +31% and +36% per 10% increase in P, and declined with reduced P at lower rates of around −20% and −17% per 10% decrease in P. Annual runoff and maximum streamflow declined by around 4% and 6% respectively per 1 ℃ of warming. Annual ET increased by 7% per 1 ℃ of warming, a much stronger sensitivity than the 1% increase per 10% increase in P. ET

changes with T controlled the streamflow volume sensitivity to T. The onset of spring snowmelt advanced by 6 days per +1 ℃ warming and the snow-cover duration declined by 10 days per +1 ℃ warming; both showed stronger sensitivities to warming than to perturbed P. Change of centre of mass timing (CMT) of annual runoff per +1 ℃ warming was close (but inverse) to that per 10% increase in P. Runoff coefficient (RC) was more sensitive to perturbed P(+16% per 10% increase in P and −15% per 10% decrease in P) than to perturbed T (−4.7% per 1 ℃ of warming).

(2) Perturbations of P and T impacted the streamflow regime in very different ways. Increasing P enhanced the intra-annual variability of basin runoff by generating substantially larger runoff volumes in the warm months (May to September) and much greater peak streamflow, whilst warming T resulted in more even distribution of monthly runoff by reducing the fractional runoff volume in April to September and the magnitudes of peak streamflow. Meanwhile, increasing P enhanced the inter-annual variability of basin runoff in the warm months, whilst rising T reduced the inter-annual variability of runoff in the warm months but increased the inter-annual variability of runoff in the cold months. On the other hand, increasing P reduced the relative contributions of spring and winter runoff to the annual runoff but enhanced the fractional contribution of summer runoff. In contrast, rising T reduced the fractional contribution of summer runoff but increased fractions of runoff generation in the autumn and winter seasons. Both P and T increases promoted a higher contribution of subsurface interflow to total runoff, but the contributions of runoff components tended to show higher sensitivities to perturbed P than to perturbed T.

(3) Effects of T warming on annual and seasonal runoff, runoff components and basin snow accumulation could sometimes be compensated for by the effects of increasing P. The annual runoff, runoff components including subsurface interflow and rainfall overland flow, and the seasonal runoff from autumn showed stronger sensitivities to changing P than to warming. Thus, changes of these variables caused by warming from 1 ℃ to 6 ℃ could be compensated for by the changes forced by small increases of <10% in P. Variables such as runoff coefficient, groundwater flow, and seasonal runoff from spring, summer, and winter presented similar sensitivities to both changing P and T. Reductions of these variables caused by the maximum warming of 6 ℃ could be compensated for by the increases generated by 17%-20% higher P. Other variables including the CMT of annual runoff and snow variables such as peak SWE, snow-cover duration, annual snow sublimation, and snowmelt overland flow, were more sensitive to warming than to perturbed P. The maximum increase in P (+30%) could only compensate for the changes in these variables caused by warming of less than 4 ℃.

## CRediT authorship contribution statement

**Zhihua He:** Conceptualization, Methodology, Writing – original draft, Writing - review & editing. **John W. Pomeroy:** Conceptualization, Methodology, Writing – original draft, Writing - review & editing. **Xing Fang:** Writing – original draft, Writing - review & editing. **Amber Peterson:** Writing - review & editing.

## Declaration of Competing Interest

The authors declare that they have no known competing financial interests or personal relationships that could have appeared to influence the work reported in this paper.

## Acknowledgements

This work is funded by the Global Water Futures program. The authors gratefully acknowledge all the researchers who have collected field observations in the White Gull Creek basin in the BOREAS and BERMS studies since the early 1990 s, especially Dr. Warren Helgason and Dr. Alan Barr of the University of Saskatchewan.

## References

Agriculture and Agri-Food Canada, 2015. National ecological framework. Accessed 10 June 2016. [Available online at. http://sis.agr.gc.ca/cansis/nsdb/ecostrat/index.html.].

Ahmed, H., Helgason, W., Barr, A., Black, T., 2020. Hydrometeorological observations at three boreal forest sites (aspen, jack pine, and black spruce) located in central Saskatchewan, Canada [Dataset]. Federated Research Data Repository. https://doi.org/10.20383/101.0292.

Ayers, H.D., 1959. Influence of soil profile and vegetation characteristics on net rainfall supply to runoff. In: Proceedings of Hydrology Symposium No.1: Spillway Design Floods, pp. 198–205.

Aygün, O., Kinnard, C., Campeau, S., Krogh, S.A., 2020. Shifting hydrological processes in a Canadian agroforested catchment due to a warmer and wetter climate. Water 12 (3), 739. https://doi.org/10.3390/w12030739.

Barr, A.G., van der Kamp, G., Black, T.A., McCaughey, J.H., Nesic, Z., 2012. Energy balance closure at the BERMS flux towers in relation to the water balance of the White Gull Creek watershed 1999–2009. Agric. For. Meteorol. 153, 3–13. https://doi.org/10.1016/j.agrformet.2011.05.017.

Bartlett, P.A., MacKay, M.D., Verseghy, D.L., 2006. Modified snow algorithms in the Canadian Land Surface Scheme: Model runs and sensitivity analysis at three boreal forest stands. Atmos. Ocean 44 (3), 207–222.

Bonan, G.B., 2008. Forests and climate change: forcings, feedbacks, and the climate benefits of forests. Science 320 (5882), 1444–1449. https://doi.org/10.1126/science:1155121.

Boulanger, Y., Taylor, A.R., Price, D.T., Cyr, D., McGarrigle, E., Rammer, W., Sainte-Marie, G., Beaudoin, A., Guindon, L., Mansuy, N., 2016. Climate change impacts on forest landscapes along the Canadian southern boreal forest transition zone. Landscape Ecol. 32 (7), 1415–1431.

Brandt, J.P., Flannigan, M.D., Maynard, D.G., Thompson, I.D., Volney, W.J.A., 2013. An introduction to Canada's boreal zone: ecosystem processes, health, sustainability, and environmental issues. Environ. Rev. 21 (4), 207–226. https://doi.org/10.1139/er-2013-0040.

Brown, R.D., Fang, B., Mudryk, L., 2019. Update of Canadian Historical Snow Survey Data and Analysis of Snow Water Equivalent Trends, 1967–2016. Atmos. - Ocean 57 (2), 149–156. https://doi.org/10.1080/07055900.2019.1598843.

Brown, S.M., Petrone, R.M., Chasmer, L., Mendoza, C., Lazerjan, M.S., Landhäusser, S.M., Silins, U., Leach, J., Devito, K.J., 2014. Atmospheric and soil moisture controls on evapotranspiration from above and within a western boreal plain aspen forest. Hydrol. Processes. 28 (15), 4449–4462.

Bush, E. and Lemmen, D.S., editors, 2019. Canada's Changing Climate Report; Government of Canada, Ottawa, ON. 444 p.

Buttle, J.M., Creed, I.F., Pomeroy, J.W., 2000. Advances in Canadian forest hydrology, 1995–1998. Hydrol. Processes 14 (9), 1551–1578.

Buttle, J M, Metcalfe, R A, 2000. Boreal forest disturbance and streamflow response, northeastern Ontario. Canadian Journal of Fisheries and Aquatic Sciences 57 (S2), 5–18.

Changwei, X., Gough, W.A., 2013. A simple thaw-freeze algorithm for a multi-layered soil using the Stefan equation. Permafrost Periglac. 24 (3), 252–260. https://doi.org/10.1002/ppp.1770.

Chen, Jing M., Rich, Paul M., Gower, Stith T., Norman, John M., Plummer, Steven, 1997. Leaf area index of boreal forests: theory, techniques, and measurements. J. Geophys. Res. 102 (D24), 29429–29443.

Chow, V.T., 1964. Handbook of Applied Hydrology. McGraw-Hill, New York, p. 1495.

Clark, C. O., 1945. Storage and the unit hydrograph. Proceedings of the American Society of Civil Engineering, 69, 1419-1447.

Davison, B., Pietroniro, A., Fortin, V., Leconte, R., Mamo, M., Yau, M. K., 2016. What is missing from the Prescription of Hydrology for Land Surface Schemes? J. Hydrometeorol., 17, 2013–2039.https://doi.org/10.1175/JHM-D-15-0172.1.

ECCC [Environment and Climate Change Canada] (2016): Climate data and scenarios for Canada: Synthesis of recent observation and modelling results. Cat. No.: En84-132/2016E-PDF.

Elliott, J.A., Toth, B.M., Granger, R.J., Pomeroy, J.W., 1998. Soil moisture storage in mature and replanted sub-humid boreal forest stands. Can. J. Soil Sci. 78 (1), 17–27. https://doi.org/10.4141/S97-021.

Ellis, C.R., Pomeroy, J.W., Brown, T., MacDonald, J., 2010. Simulation of snow accumulation and melt in needle leaf forest environments. Hydrol. Earth Syst. Sc. 14, 925–940. https://doi.org/10.5194/hess-14-925-2010.

Endalamaw, A., Bolton, W.R., Young-Robertson, J.M., Morton, D., Hinzman, L., Nijssen, B., 2017. Towards improved parameterization of a macroscale hydrologic model in a discontinuous permafrost boreal forest ecosystem. Hydrol. Earth Syst. Sc. 21, 4663–4680. https://doi.org/10.5194/hess-21-4663-2017.

Euskirchen, E.S., McGuire, A.D., Chapin III, F.S., Rupp, T.S., 2010. The changing effects of Alaska's boreal forests on the climate system. Can. J. Forest Res. 40, 1336–1346. https://doi.org/10.1139/X09-209.

Fang, X., Pomeroy, J.W., Westbrook, C.J., Guo, X., Minke, A.G., Brown, T., 2010. Prediction of snowmelt derived streamflow in a wetland dominated prairie basin. Hydrol. Earth Syst. Sc. 14 (6), 991–1006.

Fang, X., Pomeroy, J.W., Ellis, C.R., MacDonald, M.K., DeBeer, C.M., Brown, T., 2013. Multi-variable evaluation of hydrological model predictions for a headwater basin in the Canadian Rocky Mountains. Hydrol. Earth Syst. Sc. 17 (4), 1635–1659.

Garnier, B.J., Ohmura, Atsumu, 1970. The evaluation of surface variations in solar radiation income. Sol. Energy 13 (1), 21–34.

Gauthier, S., Bernier, P., Kuuluvainen, T., Shvidenko, A.Z., Schepaschenko, D.G., 2015. Boreal forest health and global change. Science 349 (6250), 819–822. https://doi.org/10.1126/science:aaa9092.

Gelfan, A.N., Pomeroy, J.W., Kuchment, L.S., 2004. Modeling Forest Cover Influences on Snow Accumulation, Sublimation, and Melt. J. Hydrometeorol. 5, 785–803. https://doi.org/10.1175/1525-7541(2004)005<0785:MFCIOS>2.0.CO;2.

Granger, R. J., Gray, D. M., 1990. A net radiation model for calculating daily snowmelt in open environments. Nordic Hydrology, 21, 217 – 234.

Granger, R.J., Pomeroy, J.W., 1997. Sustainability of the western Canadian boreal forest under changing hydrological conditions. II. Summer energy and water use. IAHS-AISH Publ. 240, 243–249.

Gray, D.M., Toth, Brenda, Zhao, Litong, Pomeroy, J.W., Granger, R.J., 2001. Estimating areal snowmelt infiltration into frozen soils. Hydrol. Process. 15 (16), 3095–3111. https://doi.org/10.1002/(ISSN)1099-108510.1002/hyp.v15:1610.1002/hyp.320.

Harder, P., Pomeroy, J., 2013. Estimating precipitation phase using a phycrometric energy balance method. Hydrol. Processes 27, 1901–1914. https://doi.org/10.1002/hyp.9799.

Hardy, J.P., Davis, R.E., Jordan, R., Ni, W., Woodcock, C.E., 1998. Snow ablation modelling in a mature aspen stand of the boreal forest. Hydrol. Processes 12 (10-11), 1763–1778.

He, Z., 2021. Sensitivities of Hydrological Processes to Climate Changes in a Central Asian Glacierized Basin. Front. Water 3, 683146. https://doi.org/10.3389/frwa.2021.683146.

Hedstrom, N.R., Pomeroy, J.W., 1998. Measurements and modeling of snow interception in the boreal forest. Hydrol. Processes 12, 1611–1625. https://doi.org/10.1002/(SICI)1099-1085(199808/09)12:10/11<1611::AID-HYP684>3.0.CO;2-4.

Holmberg, M., Futter, M. N., Kotamäki, N., Fronzek, S., Forsius, M., Kiuru, P., Pirttioja, N., Rasmus, K., Starr, M., Vuorenmaa, J., 2014. Effects of changing climate on the hydrology of a boreal catchment and lake DOC—Probabilistic assessment of a dynamic model chain, Boreal Environ. Res., 19(suppl. A), 66–82.

Ireson, A.M., Barr, A.G., Johnstone, J.F., Mamet, S.D., van der Kamp, G., Whitfield, C.J., Michel, N.L., North, R.L., Westbrook, C.J., DeBeer, C., Chun, K.P., Nazemi, A., Sagin, J., 2015. The changing water cycle: The Boreal Plains ecozone of Western Canada. Wiley Interdisciplinary Reviews-Water 2 (5), 505–521. https://doi.org/10.1002/wat2.2015.2.issue-510.1002/wat2.1098.

Kozii, N., Laudon, H., Löfvenius, M.O., Hasselquist, N.J., 2017. Increasing water losses from snow captured in the canopy of boreal forests: A case study using a 30 year data set. Hydrol. Processes 31, 3558–3567. https://doi.org/10.1002/hyp.11277.

Krogh, S.A., Pomeroy, J.W., Marsh, P., 2017. Diagnosis of the hydrology of a small Arctic basin at the tundra-taiga transition using a physically based hydrological model. J. Hydrol. 550, 685–703. https://doi.org/10.1016/j.jhydrol.2017.05.042.

Li, Y., Li, Z., Zhang, Z., Chen, L., Kurkute, S., Scaff, L., Pan, X., 2019. High-resolution regional climate modeling and projection over western Canada using a weather research forecasting model with a pseudo-global warming approach. Hydrol. Earth Syst. Sci. 23(11), 4635–4659. https ://doi.org/10.5194/hess-23-4635-2019.

López-Moreno, J.I., Pomeroy, J.W, Revuelto, J., Vicente-Serrano, S.M., 2012. Response of snow processes to climate change: spatial variability in a small basin in the Spanish Pyrenees. Hydrol. Processes 27 (18), 2637–2650. https://doi.org/10.1002/hyp.v27.1810.1002/hyp.9408.

Luce, C.H., Tarboton, D.G., 2010. Evaluation of alternative formulae for calculation of surface temperature in snowmelt models using frequency analysis of temperature observations. Hydrol. Earth Syst. Sc. 14 (3), 535–543.

Marks, Danny, Kimball, John, Tingey, Dave, Link, Tim, 1998. The sensitivity of snowmelt processes to climate conditions and forest cover during rain-on-snow: a case study of the 1996 Pacific Northwest flood. Hydrol. Processes 12 (10-11), 1569–1587.

Metcalfe, R.A., Buttle, J.M., 2001. Soil partitioning and surface store controls on spring runoff from a boreal forest peatland basin in north-central Manitoba. Canada. Hydrol. Process. 15 (12), 2305–2324.

Monteith, J.L., 1965. In: Evaporation and environment. In State and Movement of Water in Living Organisms. Cambridge University Press, Cambridge, pp. 205–234.

Nash, J.E., Sutcliffe, J.V., 1970. River flow forecasting through conceptual models. Part I—A discussion of principles. J. Hydrol. 10 (3), 282–290.

Nelson, T.A., Coops, N.C., Wulder, M.A., Perez, L., Fitterer, J., Powers, R., Fontana, F., 2014. Predicting climate change impacts to the canadian boreal forest. Diversity 6, 133–157. https://doi.org/10.3390/d6010133.

Nijssen, Bart, Lettenmaier, Dennis P., 2002. Water balance dynamics of a boreal forest watershed: White Gull Creek basin, 1994–1996. Water Resour. Res. 38 (11), 37-1–37-12. https://doi.org/10.1029/2001WR000699.

Peng, Changhui, Ma, Zhihai, Lei, Xiangdong, Zhu, Qiuan, Chen, Huai, Wang, Weifeng, Liu, Shirong, Li, Weizhong, Fang, Xiuqin, Zhou, Xiaolu, 2011. A drought-induced pervasive increase in tree mortality across Canada's boreal forests. Nat. Clim. Change 1 (9), 467–471. https://doi.org/10.1038/nclimate1293.

Pomeroy, J., Fang, X., Ellis, C., 2012. Sensitivity of snowmelt hydrology in Marmot Creek, Alberta, to forest cover disturbance. Hydrol. Process. 26, 1891–1904. https://doi.org/10.1002/hyp.9248.

Pomeroy, J.W., Granger, R.J., 1997. Sustainability of the western Canadian boreal forest under changing hydrological conditions — I: snow accumulation and ablation. In: Rosjberg, D., Boutayeb, N., Gustard, A., Kundzewicz, Z., Rasmussen, P. (Eds.), Sustainability of water resources under increasing uncertainty. IAHS Press, Wallingford, UK, pp. 207–242.

Pomeroy, J.W., Granger, R., Pietroniro, A., Elliott, J., Toth, B., Hedstrom, N., 1999. Classification of the boreal forest for hydrological processes, in Proceedings of the Ninth International Boreal Forest Research Association Conference. In: Woxholtt, S. (Ed.), Aktuelt fraskogforskningen, Norsk institutt for skogforskning, Norw. Institute, Oslo, pp. 49–59.

Pomeroy, J.W., Gray, D.M., 1995. Snow cover Accumulation, Relocation and Management, Science Report No. 7, 144 pp..

Pomeroy, J.W., Parviainen, J., Hedstrom, N.R., Gray, D.M., 1998. Coupled modeling of forest snow interception and sublimation. Hydrol. Processes 12, 2317–2337.

Pomeroy, J.W., Gray, D.M., Hedstrom, N.R., Janowicz, J.R., 2002. Prediction of seasonal snow accumulation in cold climate forests. Hydrol. Processes 16 (18), 3543–3558.

Pomeroy, J.W., Gray, D.M., Brown, T., Hedstrom, N.R., Quinton, W.L., Granger, R.J., Carey, S.K., 2007. The Cold Regions Hydrological Model, a platform for basing process representation and model structure on physical evidence. Hydrol. Processes 21 (19), 2650–2667. https://doi.org/10.1002/(ISSN)1099-108510.1002/hyp.v21:1910.1002/hyp.6787.

Pomeroy, John W., Marks, Danny, Link, Tim, Ellis, Chad, Hardy, Janet, Rowlands, Aled, Granger, Raoul, 2009. The impact of coniferous forest temperature on incoming longwave radiation to melting snow. Hydrol. Processes 23 (17), 2513–2525. https://doi.org/10.1002/hyp.v23:1710.1002/hyp.7325.

Pomeroy, J.W., Fang, X., Marks, D., 2016. A cold rain on snow event in the Canadian Rockies—characteristics and diagnosis. Hydrological Processes 30, 2899–2914. https://doi.org/10.1002/hyp.10905.

Pomeroy, J.W., Gray, D.M., Landine, P.G., 1993. The Prairie Blowing Snow Model: characteristics, validation, operation. J. Hydrol. 144, 165–192. https://doi.org/10.1016/0022-1694 (93)90171-5.

Pomeroy, J.W., Li, L., 2000. Prairie and Arctic areal snow cover mass balance using a blowing snow model. J. Geophys. Res. 105 (D21), 26619–26634.

Price, D.T., Alfaro, R.I., Brown, K.J., Flannigan, M.D., Fleming, R.A., Hogg, E.H., Girardin, M.P., Lakusta, T., Johnston, M., McKenney, D.W., Pedlar, J.H., Stratton, T., Sturrock, R.N., Thompson, I.D., Trofymow, J.A., Venier, L.A., 2013. Anticipating the consequences of climate change for Canada's boreal forest ecosystems1. Environ. Rev. 21 (4), 322–365. https://doi.org/10.1139/er-2013-0042.

PRIESTLEY, C.H.B., TAYLOR, R.J., 1972. On the assessment of surface heat flux and evaporation using large-scale parameters. Mon. Weather Rev. 100 (2), 81–92.

Rasmus, S., Gustafsson, D., Koivusalo, H., Laurén, A., Grelle, A., Kauppinen, O.K., Lagnvall, O., Lindroth, A., Rasmus, K., Svensson, M., Weslien, P., 2013. Estimation of winter leaf area index and sky view fraction for snow modelling in boreal coniferous forests: consequences on snow mass and energy balance. Hydrol. Processes. 27, 2876–2891.

Rasouli, K., Pomeroy, J.W., Janowicz, J.R., Carey, S.K., Williams, T.J., 2014. Hydrological sensitivity of a northern mountain basin to climate change. Hydrol. Processes 28, 4191–4208. https://doi.org/10.1002/hyp.10244.

Rasouli, K., Pomeroy, J.W., Marks, D.G., 2015. Snowpack sensitivity to perturbed climate in a cool mid-latitude mountain catchment. Hydrol. Process. 29, 3925–3940. https://doi.org/10.1002/hyp.10587.

Rasouli, K., Pomeroy, J.W., Whitfield, P.H., 2019. Are the effects of vegetation and soil changes as important as climate change impacts on hydrological processes? Hydrol. Earth Syst. Sci. 23, 4933–4954. https://doi.org/10.5194/hess-23-4933-2019.

Schmidt, R.A., Gluns, David R., 1991. Snowfall interception on branches of three conifer species. Can. J. Forest Res. 21 (8), 1262–1269.

Sellers, Piers J., Hall, Forrest G., Kelly, Robert D., Black, Andrew, Baldocchi, Dennis, Berry, Joe, Ryan, Michael, Ranson, K. Jon, Crill, Patrick M., Lettenmaier, Dennis P., Margolis, Hank, Cihlar, Josef, Newcomer, Jeffrey, Fitzjarrald, David, Jarvis, Paul G., Gower, Stith T., Halliwell, David, Williams, Darrel, Goodison, Barry, Wickland, Diane E., Guertin, Florian E., 1997. BOREAS in 1997: experiment overview, scientificresults, and future directions. Journal of Geophysical Research 102 (D24), 28731–28769.

Sicart, J.E., Pomeroy, J.W., Essery, R.L.H., Bewley, D., 2006. Incoming longwave radiation to melting snow: observations, sensitivity and estimation in northern environments. Hydrol. Processes 20 (17), 3697–3708. https://doi.org/10.1002/(ISSN)1099-108510.1002/hyp.v20:1710.1002/hyp.6383.

Sulla-Menashe, D., Woodcock, C. E., Friedl, M. A., 2018. Canadian boreal forest greening and browning trends: An analysis of biogeographic patterns and the relative roles of disturbance versus climate drivers. Environ. Res. Lett. 13. https://doi.org/10.1088/1748-9326/aa9b88.

Verseghy, D.L., 1991. CLASS-A Canadian land surface scheme for GCMs. I. soil model. Int. J. Climatol. 11 (2), 111–133.

Williams, T. J., Pomeroy, J. W., Janowicz, J. R., Carey, S. K., Rasouli, K., Quinton, W. L., 2015. A radiative–conductive–convective approach to calculate thaw season ground surface temperatures for modelling frost table dynamics. Hydrol. Processes, 29(18), 3954–3965.https://doi.org/10.1002/hyp.10573.

Woo, Ming-ko, Thorne, Robin, Szeto, Kit, Yang, Daqing, 2008. Streamflow hydrology in the boreal region under the influences of climate and human interference. Philosophical Transactions of the Royal Society B—Biological Sciences 363 (1501), 2249–2258.

Zhang, X., Flato, G., Kirchmeier-Young, M., Vincent, L., Wan, H., Wang, X., Rong, R., Fyfe, J., Li, G., Kharin, V.V., 2019. Changes in Temperature and Precipitation Across Canada; Chapter 4 in Bush, E. and Lemmen, D.S. (Eds.) Canada's Changing Climate Report. Government of Canada, Ottawa, Ontario, pp 112-193.

Zhao, Litong, Gray, D.M., 1999. Estimating snowmelt infiltration into frozen soils. Hydrol. Processes 13 (12-13), 1827–1842.